AGU PUBLICATIONS

Geochemistry, Geophysics, Geosystems

RESEARCH ARTICLE
10.1002/2015GC005931

Key Points:
- New Northeast Greenland bathymetry reveals seafloor morphological features
- A new paleo-ice flow reconstruction for Northeast Greenland
- Refined water mass pathways to Northeast Greenland marine-terminating glaciers

Supporting Information:
- Supporting information S1

Correspondence to:
J. E. Arndt,
Jan.Erik.Arndt@awi.de

Citation:
Arndt, J. E., W. Jokat, B. Dorschel, R. Myklebust, J. A. Dowdeswell, and J. Evans (2015), A new bathymetry of the Northeast Greenland continental shelf: Constraints on glacial and other processes, *Geochem. Geophys. Geosyst.*, *16*, 3733–3753, doi:10.1002/2015GC005931.

Received 27 MAY 2015
Accepted 9 OCT 2015
Accepted article online 13 OCT 2015
Published online 30 OCT 2015

A new bathymetry of the Northeast Greenland continental shelf: Constraints on glacial and other processes

Jan Erik Arndt[1], Wilfried Jokat[1], Boris Dorschel[1], Reidun Myklebust[2], Julian A. Dowdeswell[3], and Jeffrey Evans[4]

[1]Alfred Wegener Institute, Helmholtz Centre for Polar and Marine Research, Bremerhaven, Germany, [2]TGS-NOPEC Geophysical Company ASA, Asker, Norway, [3]Scott Polar Research Institute, University of Cambridge, Cambridge, UK, [4]Department of Geography, Loughborough University, Loughborough, UK

Abstract A new digital bathymetric model (DBM) for the Northeast Greenland (NEG) continental shelf (74°N–81°N) is presented. The DBM has a grid cell size of 250 m × 250 m and incorporates bathymetric data from 30 multibeam cruises, more than 20 single-beam cruises and first reflector depths from industrial seismic lines. The new DBM substantially improves the bathymetry compared to older models. The DBM not only allows a better delineation of previously known seafloor morphology but, in addition, reveals the presence of previously unmapped morphological features including glacially derived troughs, fjords, grounding-zone wedges, and lateral moraines. These submarine landforms are used to infer the past extent and ice-flow dynamics of the Greenland Ice Sheet during the last full-glacial period of the Quaternary and subsequent ice retreat across the continental shelf. The DBM reveals cross-shelf bathymetric troughs that may enable the inflow of warm Atlantic water masses across the shelf, driving enhanced basal melting of the marine-terminating outlet glaciers draining the ice sheet to the coast in Northeast Greenland. Knolls, sinks, and hummocky seafloor on the middle shelf are also suggested to be related to salt diapirism. North-south-orientated elongate depressions are identified that probably relate to ice-marginal processes in combination with erosion caused by the East Greenland Current. A single guyot-like peak has been discovered and is interpreted to have been produced during a volcanic event approximately 55 Ma ago.

1. Introduction

The Northeast Greenland (NEG) continental shelf (20°W–5°W and 74°N–81°N) is the broadest shelf along the Greenland margin, extending more than 300 km from the coastline (Figure 1). It is bounded to the east by the Fram Strait, the only deep water connection between Arctic Ocean and lower-latitude seas, and to the west by the East Greenland coastline that consists of fjords, islands, and marine-terminating glaciers. Nioghalvfjerdsfjorden Glacier (also referred to as 79°-Glacier), Zachariae Isstrøm, Storstrømmen, and L. Bistrup Bræ (Figure 1b) are the major ice streams of the Greenland Ice Sheet in our study area, of which the former three are part of the Northeast Greenland ice stream (Figure 1; NEGIS) that extends up to ~700 km inland [*Joughin et al.*, 2001]. In total, these ice streams drain about 20% of the Greenland Ice Sheet [*Zwally et al.*, 2012]. Over the past few decades, the NEG area of the ice sheet has been thought to be relatively stable compared to other parts of Greenland [*Joughin et al.*, 2010; *Rignot and Kanagaratnam*, 2006]. Recent studies, however, have shown increased ice-sheet thinning in this area [*Helm et al.*, 2014; *Khan et al.*, 2014]. During the late Quaternary, the extent of the NEG glaciers has experienced great variability. For example, 79°-Glacier today has a fringing ice shelf approximately 80 km long and 20 km wide [*Mayer et al.*, 2000]. In the early-mid Holocene, from 7.7 to 4.5 ka, this ice shelf was not present [*Bennike and Weidick*, 2001]. In contrast, high-resolution bathymetric observations of submarine glacial features demonstrate that the ice sheet extended onto the continental shelf [*Evans et al.*, 2009; *Winkelmann et al.*, 2010] and possibly reached the shelf edge 300 km to the east during the Last Glacial Maximum (LGM) [*Bennike and Weidick*, 2001]. However, the glacial history of the NEG continental shelf remains poorly known because few records of glacial geomorphology and sediments are available and more constraints on past ice-sheet dynamics are required to understand ice-sheet response in a changing climate. With its exceptional width, the NEG continental shelf represents the largest possible oscillation of the Greenland Ice Sheet and thus is a key region to study past ice-sheet behavior and assess its possible contribution to full-glacial sea level fall. For several other formerly

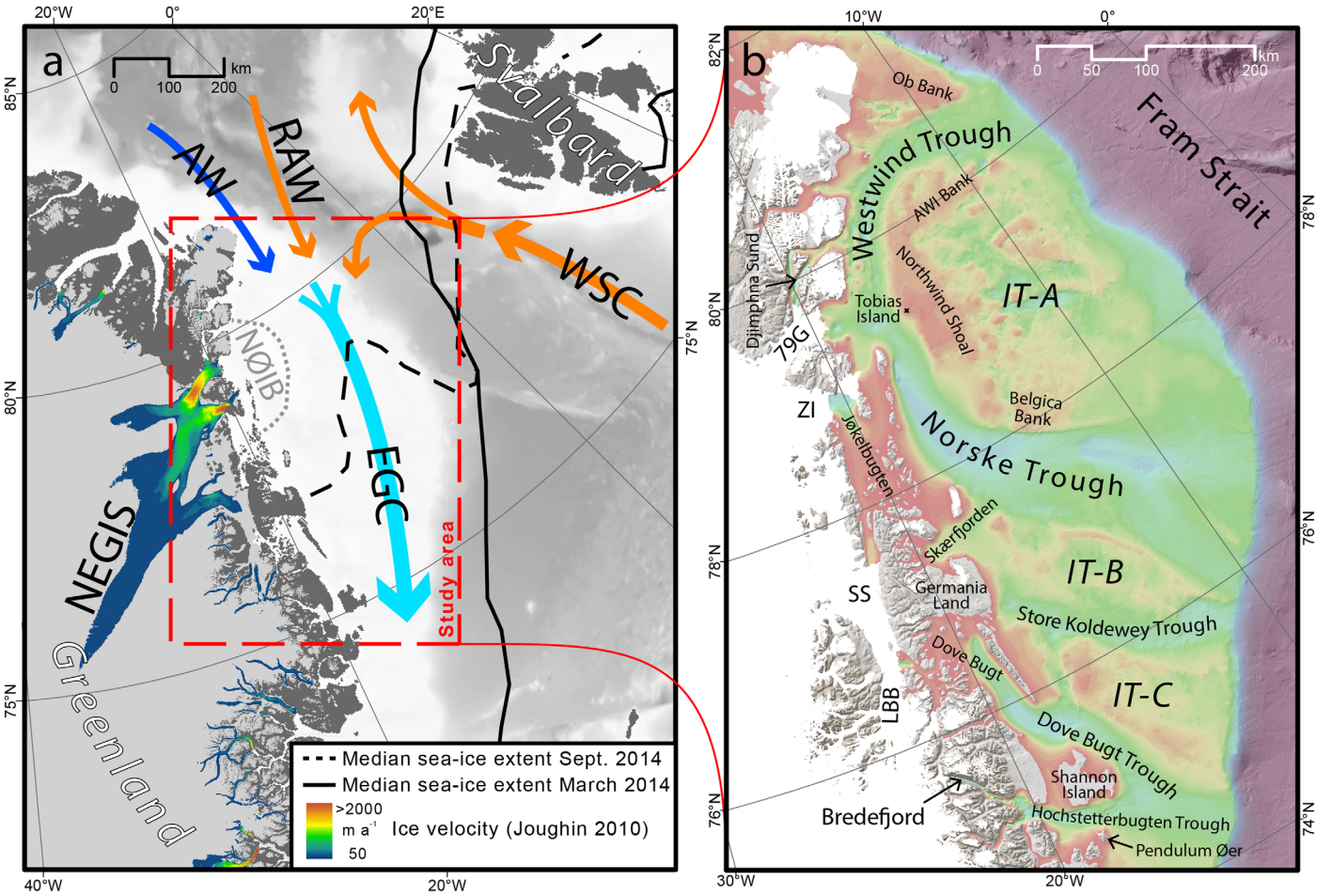

Figure 1. (a) Location map of the study area showing sea ice, glaciological, and oceanographic conditions. Ice-sheet velocities are from *Joughin et al.* [2010]. NEGIS = Northeast Greenland Ice Stream, NØIB = Norske Øer Ice Barrier, AW = Arctic Water, RAW = Return Atlantic Water, WSC = West Spitsbergen Current, and EGC = East Greenland Current. (b) Geographical names mentioned in the text; 79G = 79°-Glacier, ZI = Zachariae Isstrøm, SS = Storstrømmen, LBB = L. Bistrup Bræ, and IT = inter-trough areas.

glaciated continental shelves, new regional digital bathymetric models (DBM) have been produced recently [*Dickens et al.*, 2014; *Graham et al.*, 2011; *Nitsche et al.*, 2007], providing new insights on past ice-sheet extent and ice-stream activity through the identification and regional mapping of large-scale glacial features, such as cross-shelf troughs and grounding-zone wedges (GZWs) [e.g., *Batchelor and Dowdeswell*, 2014; *Batchelor and Dowdeswell*, 2015].

The extend and dynamics of marine-terminating glaciers or ice-streams draining the Greenland Ice Sheet are strongly dependent not only on atmospheric forcing but, additionally, on ocean circulation, which can transport relatively warm water masses to or below the ice front that enhance submarine melting at the grounding-line or underside of the floating margins [*Christoffersen et al.*, 2011; *Hellmer et al.*, 2012; *Holland et al.*, 2008]. The western part of Fram Strait and the NEG outer shelf are influenced strongly by the cold southward-flowing East Greenland Current (Figure 1a; EGC) [*Aagaard and Coachman*, 1968]. The currents on the inner shelf are still only poorly understood, with conflicting interpretations suggesting clockwise or counterclockwise water circulation [*Bourke et al.*, 1987; *Budéus and Schneider*, 1995; *Wadhams et al.*, 2006]. Nevertheless, relatively warm Atlantic water (1°C) has been observed at 79°-Glacier [*Straneo et al.*, 2012] that must have crossed the continental shelf from the east. The movement of water masses on the continental shelf is dependent, in part, on bathymetric pathways that allow the density-driven exchange of water masses. Accordingly, modeling of such systems relies on accurate knowledge of shelf bathymetry.

The geology of the NEG continental shelf is related to the highly variable and complex breakup of the North Atlantic Ocean and Fram Strait, linked to various oblique spreading processes [*Engen et al.*, 2008]. *Hamann*

et al. [2005] showed that the northern part of the NEG shelf consists predominantly of deep sedimentary basins, including areas with salt diapirism and faulting. South of 75°N, the Northeast Greenland Volcanic Province is present [*Hamann et al*., 2005]. Occasionally, these processes leave imprints in the form of unique morphological features on the seafloor. Mapping these features allows a greater horizontal resolution for geological interpretations that have previously relied on limited seismic data coverage.

The EGC continuously transports sea ice from the Arctic Ocean, resulting in year-round harsh sea ice conditions on the NEG shelf. In addition, a large area of land-fast sea ice, named Norske Øer Ice Barrier (Figure 1a), was present for decades and has recently started to break up more regularly in late summer [*Hughes et al*., 2011]. Therefore, the NEG shelf is typically inaccessible to research vessels collecting bathymetric data. This situation has changed dramatically in the last decade with periodically light sea-ice conditions even in the northern parts of NEG enabling seafloor bathymetric data to be acquired during a number of geoscience cruises.

Bathymetry data for the NEG continental shelf were first described by *Johnson and Eckhoff* [1966], indicating the wide extent of the shelf. Later, bathymetric models described trough structures on the shelf [*Perry et al*., 1980]. The most recent regional compilation was published in 1994 [*Cherkis and Vogt*, 1994]. Today, the bathymetry of the NEG shelf is best described by the International Bathymetric Chart of the Arctic Ocean (IBCAO) Version 3.0 [*Jakobsson et al*., 2012b]. These data sets, however, are outdated or, in case of IBCAO, are part of larger pan-Arctic compilations that cannot focus on relatively small regions and, thus, have more artifacts and/or missing data in comparison to a designated regional compilation.

Here we present a new regional digital bathymetric model (DBM) for the NEG continental shelf. This DBM was produced using both new and reprocessed bathymetric data. The core of the database consists of 30 cruises with multibeam echo sounder data and more than 20 cruises with single-beam echo sounder data from 1985 until the present. In addition, seismic first reflector data, echo-sounding data from an autonomous undersea vehicle (AUV), CTD maximum depths, as well as topographic under-ice data have been integrated in the database. The database was gridded at a cell size of 250 m $\times$ 250 m, which is twice as high as older models. These improvements make it possible to reveal for the first time previously unmapped seafloor landforms and to improve the resolution and description of the morphology of the NEG continental shelf. Based on the new DBM, we have mapped and described various morphological seafloor features on the NEG shelf. These provide information on the extent, pathways, and behavior of past ice streams draining the NE sector of the Greenland Ice Sheet and the location of active salt diapirism. Furthermore, the DBM serves as an important boundary condition for future oceanographic and biological research in the region.

2. Data

2.1. DBM Base Data

The compilation of the NEG DBM is based on bathymetric, topographic, and under-ice bedrock elevation data (Table 1 and Figure 2). In addition to echo-sounding data from research vessels, first reflector depth data from systematic seismic surveys have been made available by TGS and Autosub-II AUV data from mission M365 underneath Norske Øer Ice Barrier (Figure 1) [*Wadhams et al*., 2006] have been integrated.

For areas without any acoustic soundings, alternate data sets were used to constrain the water depth. Maximum depths of CTD casts were used as minimum depth information in areas where the resulting gridded depths were otherwise shallower. Furthermore, the bathymetric map of *Cherkis and Vogt* [1994] was used to infer contours close to the coast. In addition, we added inferred contours at 5 m above sea level for islands that were not represented by the topographic data sets. Some of these islands were identified offshore of the Nioghalvfjerdfjorden ice shelf edge from satellite imagery [*NASA Landsat Program*, 2000]. Tuppiap Qeqertaa (Tobias Island) on Northwind Shoal was described by *Bennike et al*. [2006] (Figure 1b). The locations of inferred contours are shown in the source identifier grid that accompanies the DBM (Figure 2 and supporting information).

2.2. Seismic Data for Interpretation

Multichannel seismic data were used from FS Polarstern cruise ARK-XV/2 (for location see Figure 4). The data were acquired in heavy ice with a 1600 m long 64-channel streamer using a tuned air gun cluster with

Table 1. Data Sets Used in the Digital Bathymetric Model[a]

Type	ID	Year	Vessel	Source	Reference
Multibeam	ARK-III/2	1985	FS Polarstern	AWI	*Klenke and Schenke* [2002]
	ARK-III/3	1985	FS Polarstern	AWI	*Klenke and Schenke* [2002]
	ARK-IV/1	1987	FS Polarstern	AWI	*Klenke and Schenke* [2002]
	ARK_IV/3	1987	FS Polarstern	AWI	*Klenke and Schenke* [2002]
	ARK-VII/1	1990	FS Polarstern	AWI	
	ARK-VII/3a	1990	FS Polarstern	AWI	*Klenke and Schenke* [2002]
	ARK-VII/3b	1990	FS Polarstern	AWI	
	ARK-VIII/3	1991	FS Polarstern	AWI	*Klenke and Schenke* [2002]
	ARK-X/1	1994	FS Polarstern	AWI	
	ARK-X/2	1994	FS Polarstern	AWI	
	ARK-XI/2	1995	FS Polarstern	AWI	*Klenke and Schenke* [2002]
	ARK-XIII/2	1997	FS Polarstern	AWI	
	ARK-XIII/3	1997	FS Polarstern	AWI	*Klenke and Schenke* [2002]
	ARK-XV/2	1999	FS Polarstern	AWI	
	ARK-XVI/1	2000	FS Polarstern	AWI	
	ARK-XVII/1	2001	FS Polarstern	AWI	
	ARK-XVIII/1	2002	FS Polarstern	AWI	
	ARK-XVIII/2	2002	FS Polarstern	AWI	
	ARK-XIX/4a	2003	FS Polarstern	AWI	
	ARK-XIX/4b	2003	FS Polarstern	AWI	
	ARK-XX/2	2004	FS Polarstern	AWI	
	ARK-XX/3	2004	FS Polarstern	AWI	
	ARK-XXIV/3	2009	FS Polarstern	AWI	*Winkelmann et al.* [2010]
	ARK-XXVII/1	2012	FS Polarstern	AWI	
	ARK-XXVIII/2	2014	FS Polarstern	AWI	
	ARK-XXVIII/3	2014	FS Polarstern	AWI	
	ARK-XXVIII/4	2014	FS Polarstern	AWI	
	LOMROG	2007	RV Oden	SU	*Jakobsson et al.* [2008, 2010]
	NEGC2008	2008	RV Oden	SU	
	JR106	2004	RRS JC Ross	SPRI	*Evans et al.* [2009]
Single beam	ARK-IX/2	1993	FS Polarstern	AWI	
	ARK-IX/3	1993	FS Polarstern	AWI	
	ARK-XIII/1	1997	FS Polarstern	AWI	
	ARK-XIV/2	1998	FS Polarstern	AWI	
	ARK-XV/1	1999	FS Polarstern	AWI	
	ARK-XV/3	1999	FS Polarstern	AWI	
	ARK-XVI/2	2000	FS Polarstern	AWI	
	ARK-XIX/2	2003	FS Polarstern	AWI	
	ARK-XX/1	2004	FS Polarstern	AWI	
	ARK-XXI/1	2005	FS Polarstern	AWI	
	ARK-XXIII/1	2008	FS Polarstern	AWI	
	ARK-XXIII/2	2008	FS Polarstern	AWI	
	ARK-XXIV/1	2009	FS Polarstern	AWI	
	ARK-XXV/1	2010	FS Polarstern	AWI	
	ARK-XXV/2	2010	FS Polarstern	AWI	
	ARK-XXVI/1	2011	FS Polarstern	AWI	
	Various cruises	2008–2014		NPI	
	1 cruise	2009	MV Arctic Sunrise	WHOI	
	PLRSEA90	1990	USCGC Polar Sea	USN	
Seismic first reflector	NEG08	2008		TGS	
	NEG09	2009		TGS	
	NEG10	2010		TGS	
	NEG11	2011		TGS	
	NEG12	2012		TGS	
	NEG13	2013		TGS	
	NEG14	2014		TGS	
	64 single shots	1998–1999		AWI	*Mayer et al.* 2000
AUV-single beam	M365	2004	Autosub-II	SPRI	*Wadhams et al.* 2006
CTD (max depths)	25 casts			NODC	
	9 casts	1998–1999		AWI	*Mayer et al.* 2000
	3 casts			NPI	
Topography	GIMP	2014		BPRC	*Howat et al.* 2014
Bedrock topography		2014		UCI	*Morlighem et al.* 2014

[a]AWI = Alfred Wegner Institute; BAS = British Antarctic Survey; BPRC = Byrd Polar Research Center; NODC = National Oceanographic Data Center; NPI = Norske Polar Institute; UCI = University of California, Irvine; USN = U.S. Naval Research Laboratory; SPRI = Scott Polar Research Institute; SU = Stockholm University; WHOI = Woods Hole Oceanographic Institute.

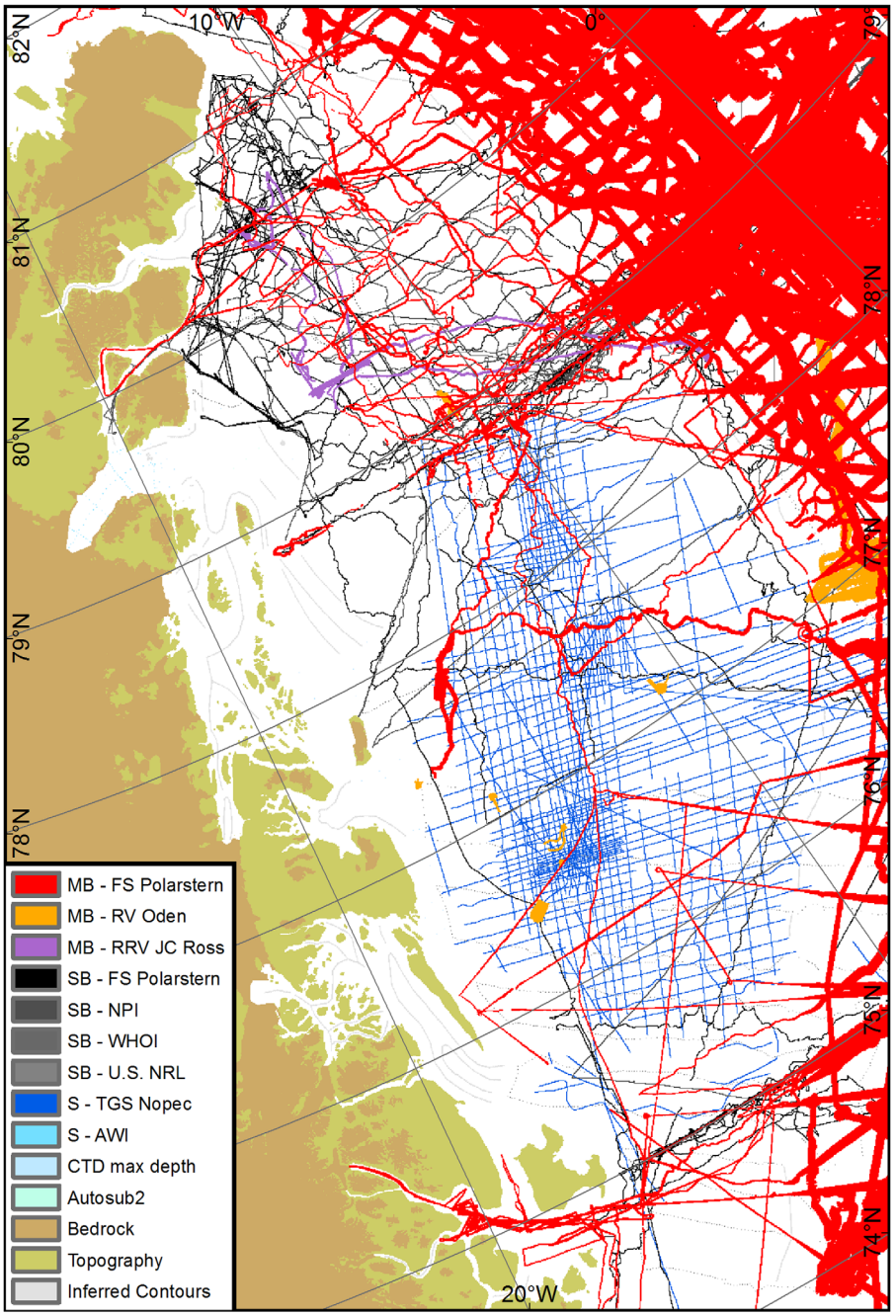

Figure 2. Bathymetric data coverage map for the Northeast Greenland shelf and deeper water showing the locations of different data sources. MB = Multibeam echo-sounding; SB = Single-beam echo-sounding; S = First reflector picked from seismic data.

a total volume of 24l (8VLF air guns). In addition, 14 sonobuoys were deployed during this cruise to better determine the seismic velocities of the subsurface.

3. Methods

3.1. Bathymetric Data Processing

All Polarstern multibeam and single-beam data were edited with CARIS HIPS and SIPS software and, finally, extracted as XYZ ASCII data. Multibeam and single-beam data from other vessels were available as partly cleaned XYZ ASCII data. All bathymetric points were checked and further cleaned with QPS Fledermaus

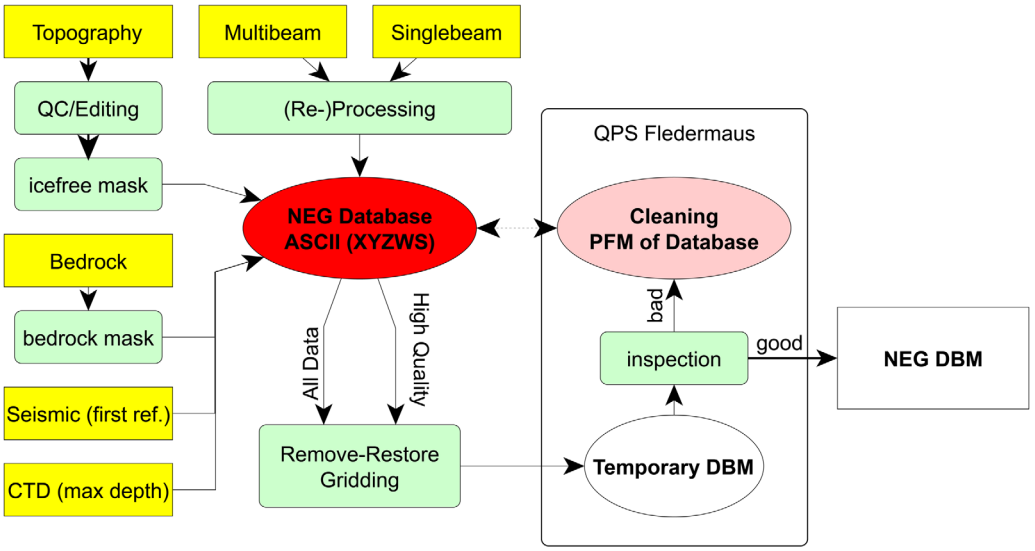

Figure 3. Scheme showing data-processing and gridding steps to produce the Northeast Greenland digital bathymetric model (NEG DBM). Yellow boxes represent data sources, green boxes are processing steps, and white boxes are the digital bathymetric models.

software using the PFM file format. Single-beam data were acquired using 1500 m/s as the standard sound velocity through water. At crossing points between single-beam data and multibeam data surveys, we were able to estimate a reasonable sound velocity from the depth differences and to correct the single-beam measurements to a common depth reference.

3.2. Topographic Data Processing

In glaciated regions, bedrock topography underneath the ice sheet is the continuation of shelf bathymetry. The onshore part of the study area comprises of ice-covered and ice-free landscapes. The Greenland Ice Mapping Project (GIMP) DEM [*Howat et al*., 2014] describes the ice sheet surface and the ice-free topography, and this was used for ice-free areas in the NEG DBM. For ice-covered areas, we used the ice-penetrating radar-derived under-ice bedrock data set from *Morlighem et al*. [2014].

The GIMP DEM showed erroneous data leading to artifacts in the surface representation in some areas (e.g., spikes or holes). Therefore, we exported the DEM as a XYZ ASCII point cloud and removed these errors using a QPS Fledermaus PFM file. The cleaned point cloud was then gridded at 200 m resolution with a spline under tension algorithm [*Smith and Wessel*, 1990] to fill the data gaps that resulted from the data editing.

The GIMP DEM and the data set from *Morlighem et al*. [2014] used ellipsoidal WGS84 altitude as the vertical reference. All bathymetric data are referenced to mean sea level. In NEG, the difference between ellipsoidal and mean sea level is approximately 30–50 m. When combining the bathymetric and land-topographic data sets, their vertical datum has to be the same. Accordingly, we transformed the vertical reference of the topographic data to the EGM2008 geoid that approximately matches mean sea level.

The elevation data sets were clipped and integrated into the DBM by applying masks on the bedrock and topographic elevation data sets. These masks were derived from the ice-covered and ice-free terrain classification masks of GIMP [*Howat et al*., 2014]. Where the GIMP DEM had erroneous areas, as mentioned above, the masks misleadingly indicated ocean grid cells. Both masks where manually cross checked for errors by comparison to satellite imagery and the adjacent topography. In the area of 79°-Glacier, and particularly on the floating ice shelf at its margin, the ice mask was modified to use the seismic measurements of *Mayer et al*. [2000] as under-ice bedrock elevation instead of the data set of *Morlighem et al*. [2014]. Finally, the masked topographic and under-ice bedrock elevation data sets were converted to XYZ ASCII. Figure 2 shows ice-free and ice-covered areas where bedrock elevation data have been used.

3.3. Gridding

The overall working scheme of the gridding process is shown in Figure 3. The XYZ ASCII files of all data sources form the data base of the NEG DBM. In addition to position and elevation (XYZ), a weighting value

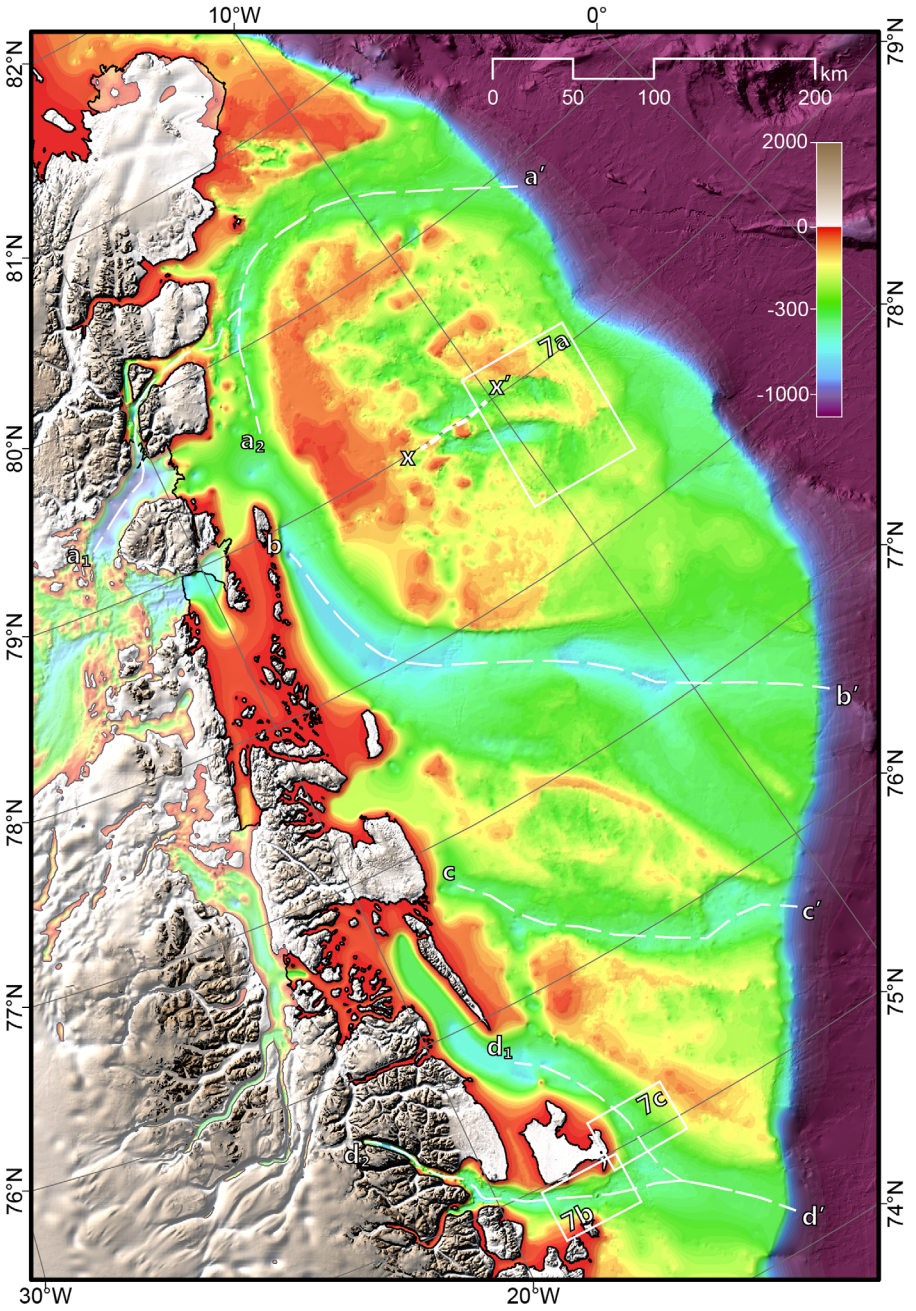

Figure 4. The new digital bathymetric model of the Northeast Greenland continental shelf based on the data shown in Table 1 and Figure 2. Black line shows the present-day coastline. White dashed lines show the locations of bathymetric profiles given in Figures 5 and 6 and the seismic line AWI-99080 in Figure 9.

and a source identification number were assigned to each data point (XYZWS) to retain information on the data source. The DBM was calculated in a polar stereographic projection with latitude of origin at 70°N and the central meridian at 45°W (EPSG:3413—WGS 84 NSIDC sea ice polar stereographic north). It covers an area of approximately 400,000 km^2 and includes the Northeast Greenland continental shelf from ~74°N to 81.5°N.

The DBM was gridded with a multiresolution gridding algorithm which has also been used in other bathymetric compilations [*Arndt et al*., 2013; *Hell and Jakobsson*, 2011; *Jakobsson et al*., 2012b]. This technique produced a smooth interpolated surface in areas with sparse data, while retaining detailed information of the seafloor morphology, where data quality and density were sufficient. Two grid cell sizes were used: a 250 m

× 250 m cell size was used as high resolution and 500 m × 500 m cell size as low resolution. To minimize artifacts at the boundary between high and low-resolution areas, we used a bending algorithm [*Arndt et al*., 2013] in a transition zone of 500 m. The resulting DBM was checked visually after gridding for artifacts in the QPS Fledermaus software. Checking the DBM and cleaning the database was repeated in an iterative process (Figure 3), until the DBM showed satisfactory results. During this process, further inferred contours were added in data gaps where the interpolation yielded unrealistic results in comparison to well-surveyed adjacent bathymetry or topography. Detailed information on the location of inferred contours can be obtained from the source identifier grid (Figure 2 and supporting information).

4. Results

The resulting bathymetric model of the NEG continental shelf and adjacent areas is presented in Figure 4. In total, 18% of the grid cells on the NEG continental shelf (down to 1000 m) are constrained directly by depth measurements. These 18% can be broken down into: 9% constrained by multibeam data, 5% by single-beam data, and 4% by other data such as seismic seafloor reflector and CTD maximum depths (Figure 2). Eighty-two percentages of the grid cells on the continental shelf remain unconstrained by depth measurements (Figure 2). Nearly 21% of the unconstrained grid cells are more than 5 km away from the nearest sounding, and 8% are more than 20 km away. Most of these unconstrained grid cells are located close to the coast, which has the lowest density sounding coverage of any location across the NEG continental shelf (Figure 2). At distances of less than 30 km from the NEG coast, only 8.6% of the grid cells are constrained directly by depth measurements.

4.1. Cross-Shelf Troughs

The new bathymetry model shows five prominent cross-shelf troughs which are deeper than the surrounding banks (Figure 4). From north to south, these are Westwind Trough, Norske Trough, Store Koldewey Trough, Dove Bugt Trough, and Hochstetterbugten Trough (Figure 1b). Together, the trough systems cover more than 40% of the NEG continental shelf with Norske Trough alone covering approximately 20% (Figure 4). The shallower shelf areas between the troughs have no names and hereafter are referred to as inter-trough areas. The area between Westwind Trough and Norske Trough is inter-trough area A (IT-A), the inter-trough area between Norske Trough and Store Koldewey Trough is inter-trough area B (IT-B), and the area between Store Koldewey Trough and Dove Bugt Trough is inter-trough area C (IT-C) (Figure 1).

4.1.1. Westwind Trough

Westwind Trough is about 300 km long with a median width of approximately 40 km. The centerline of Westwind Trough curves roughly 90° from north to east in direction (Figure 4). The edges of the trough are defined by ridges and banks on either side. On the inner shelf, an elongate ridge is present in the western part of the trough (80°N, 16.5°W). A cross section along Westwind Trough (Figure 4, a-a′; Figure 5a) shows that it has a reverse slope with a maximum water depth of more than 900 m underneath the ice shelf of 79°-Glacier and 300 m at the shelf edge. On the middle shelf, a wedge-shaped sill is present with a minimum water depth of 240 m at its easternmost position (kilometers 250–280 in Figure 5a). A sill at 160 m depth at the entrance of the Djimphna Sund fjord system is the shallowest part of the long profile.

4.1.2. Norske Trough

Norske Trough is 350 km long and its width increases from 35 km on the inner shelf to 90 km on the middle shelf and 200 km at the outer shelf (Figure 4). The centerline of Westwind Trough curves roughly 70° from a southward to a southeastward direction. Norske Trough has a reverse slope with 560 m maximum water depth at the inner shelf and 320 m at the shelf edge (Figure 5b). Close to the shelf edge, two shallower areas are present at 210 and 250 m water depth, respectively (Figure 4). On the middle shelf, a large 80 km long bathymetric sill is present where the maximum depth of the trough shallows from 490 to 360 m water depth (kilometers 120–200 in Figure 5b). Eastward of the sill, the edges of Norske Trough are defined by ridges (Figure 4 and 8). The ridge in the north is 50 km long and 30 m high. The ridge in the south is 170 km long and 100 m high.

4.1.3. Store Koldewey Trough

Store Koldewey Trough has a less pronounced trough morphology compared to the other four cross-shelf troughs (Figure 4). Its centerline is sinuous and oriented in a southeasterly direction over a length of 210 km. Its mean width is approximately 35 km. The cross section (Figure 4, c-c′; Figure 6a) shows that Store

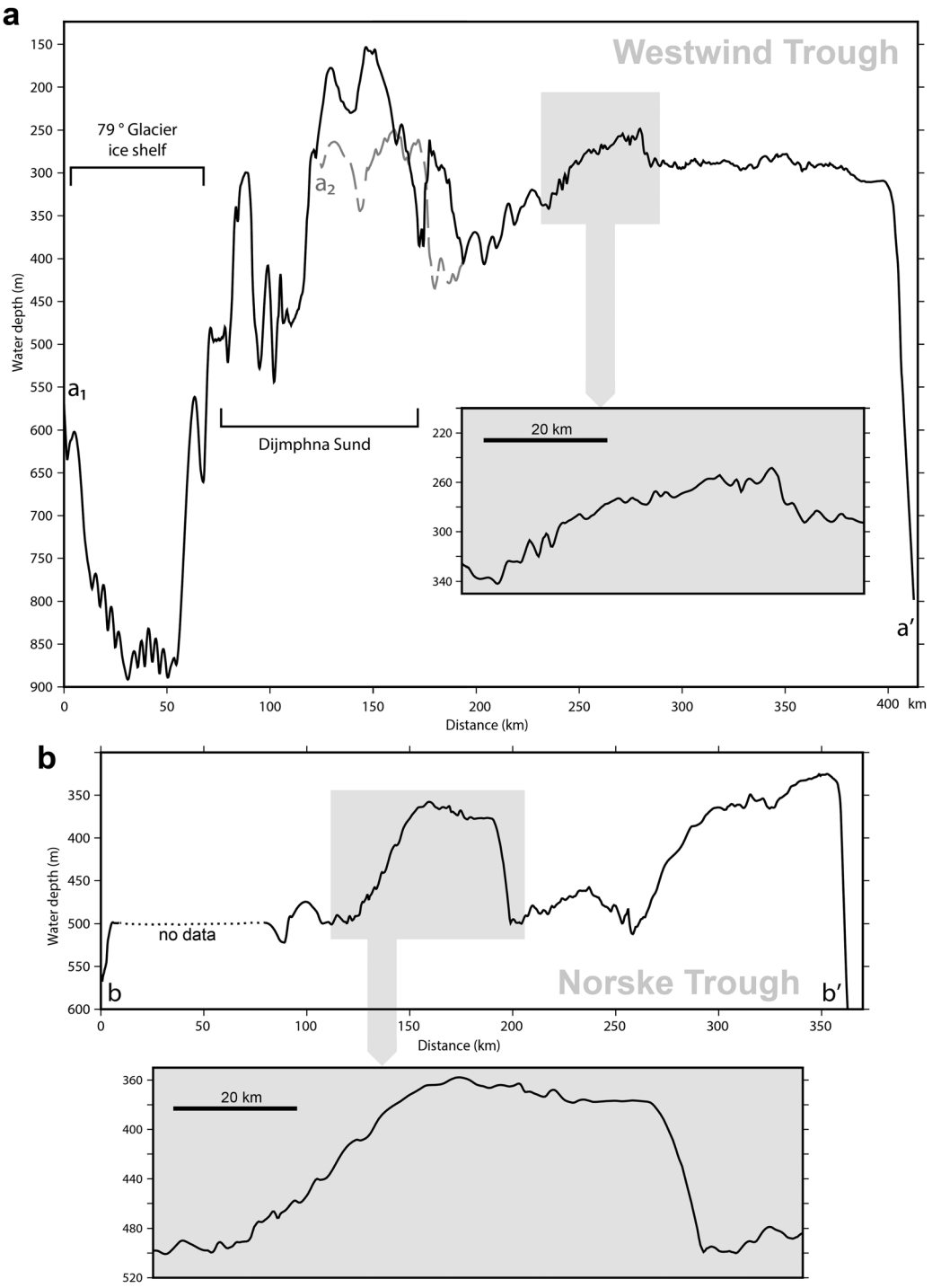

Figure 5. Bathymetric profiles of (a) Westwind Trough and (b) Norske Trough; grey insets are enlarged wedge-shaped bathymetric sills that we interpret as grounding-zone wedges; dotted line indicates that this part was not constraint by data. For locations, see Figure 4.

Koldewey Trough does not have a reverse slope but reaches its maximum depth at the shelf edge at 370 m water depth, shallowing to about 300 m on the inner shelf (Figure 8).

4.1.4. Dove Bugt Trough

Dove Bugt Trough trends southeastward until it merges with Hochstetterbugten Trough after about 120 km (Figure 4). The cross section (Figure 4, d-d′; Figure 6b) shows that Dove Bugt Trough has a reverse slope with a maximum water depth of about 490 m at the entrance to Dove Bugt and a minimum of about 300 m at the shelf edge. The northern limit of Dove Bugt Trough is defined by two banks with a ridge in between (Figures 4 and 8).

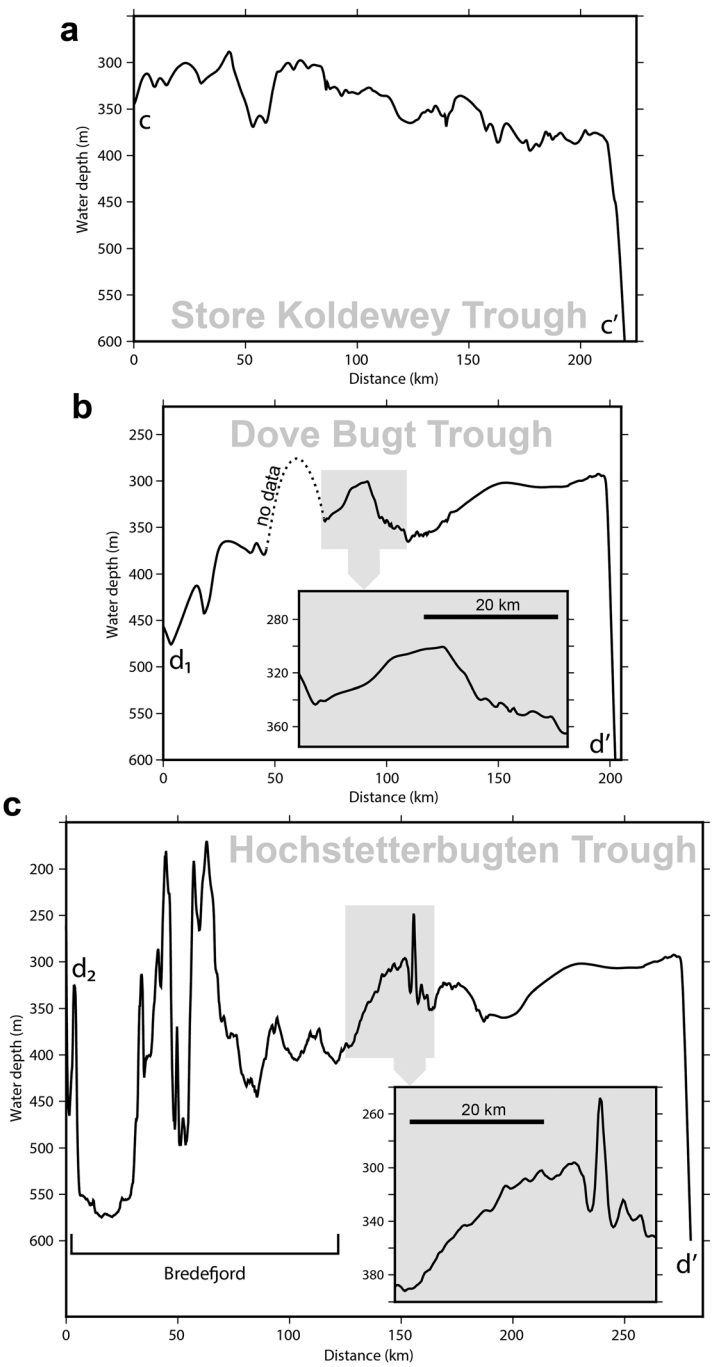

Figure 6. Bathymetric profiles of (a) Store Koldewey Trough, (b) Dove Bugt Trough, and (c) Hochstetterbugten Trough; grey insets are enlarged wedge-shaped bathymetric sills that we interpret as grounding-zone wedges; dotted line indicates that this part was not constraint by data. For location, see Figure 4.

The southern limit is defined by Shannon Island. A sill is present in Dove Bugt Trough (kilometers 70–90 in Figure 6b). The sill has a relative elevation of about 40 m and has a wedge-like relief with a steeper slope in the offshore direction (Figure 6b). In plan view, the sill has an arcuate form (Figure 7c).

4.1.5. Hochstetterbugten Trough

Hochstetterbugten Trough is the continental shelf continuation of Bredefjord (Figure 4). On the inner shelf, the trough is still constrained by a mountainous terrain and islands to the north and south until it merges with Dove Bugt Trough east of Shannon Island. Hochstetterbugten Trough has a reverse slope with a maximum depth on the inner shelf of 450 m water depth and more than 550 m in Bredefjord (Figure 6c). At the shelf break, the maximum depth is 300 m (Figure 6c). South of Shannon Island, a sill and a single peak are present in the trough (Figure 7b). The sill is 80 m high, reaching a minimum water depth of 300 m (Figure 6c). The top of the peak is relatively flat at a minimum depth of 250 m, with its flanks dropping abruptly up to 100 m into a ring-shaped depression (Figure 7b).

4.2. Shoals and Banks

The Ob Bank in the very north of the study area is generally between 50 and 100 m deep (Figures 1b, 4, and 8). At its shallowest position, it reaches approximately 40 m in depth. Northwind Shoal is the shallowest part of IT-A with average depths ranging from 20 to 80 m. Banks with an average depth of approximately 100 m are present along the trough edges north (AWI Bank) and south (Belgica Bank) of Northwind Shoal (Figures 1b, 4, and 8). Both banks are interrupted by sinks with depth changes of up to 300 m on AWI Bank and 100 m on Belgica Bank. In IT-B no banks are present. Two banks are present in IT-C, one in the west and one in the southeast. The shallowest point of the westerly bank is at about 45 m water depth. The bank is separated from the Greenland coast by an approximately 15 km wide and 200 m deep channel connecting Store Koldewey Trough with Dove Bugt Trough. The southeasterly bank is on average at 100 m depth.

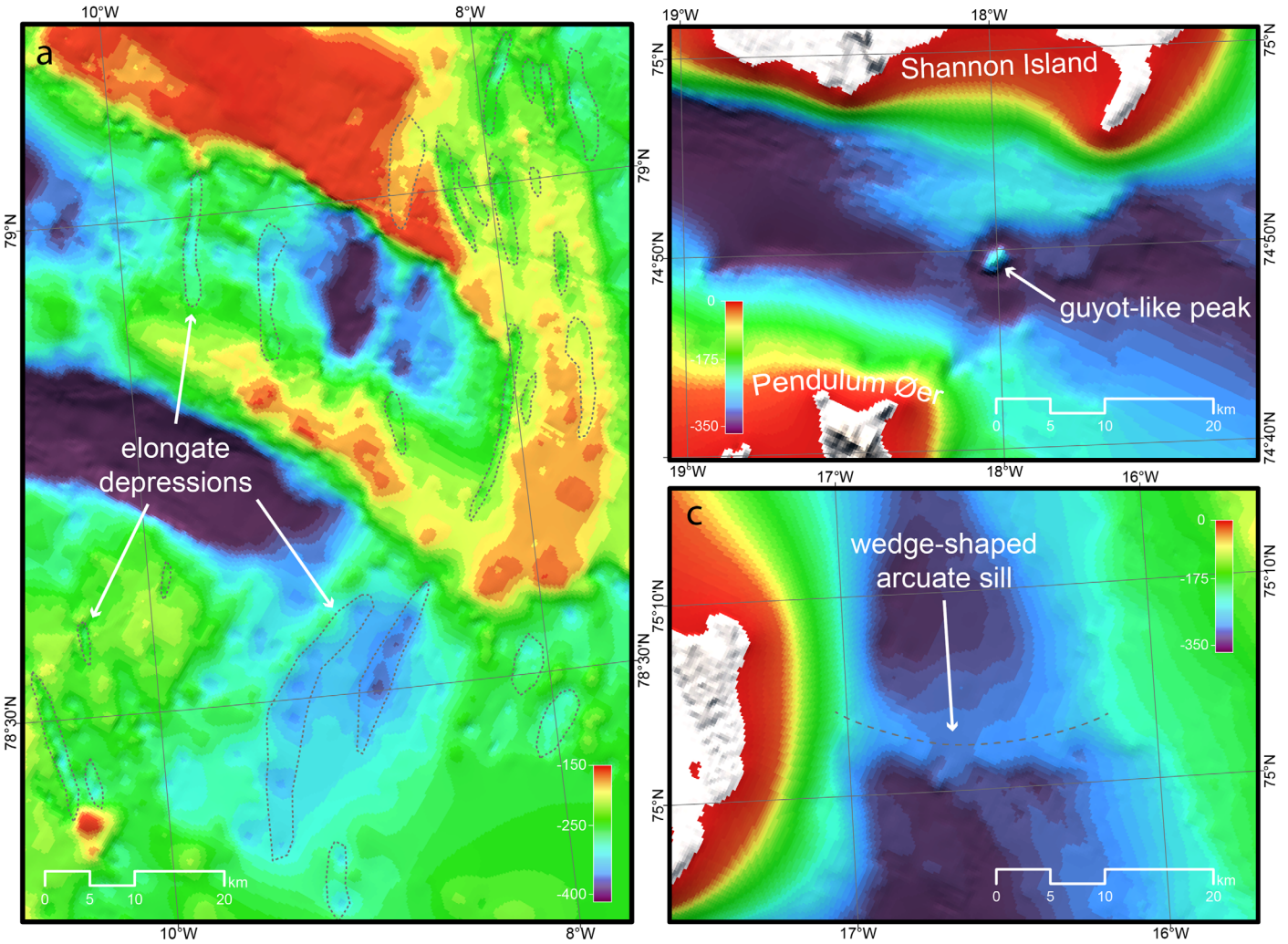

Figure 7. Detailed images of the Northeast Greenland bathymetry showing: (a) elongate depressions in inter-trough area A, (b) a guyot-like peak with a ring-shaped depression in Hochstetterbugten Trough, and (c) a wedge-shaped arcuate sill in Dove Bugt Trough. For locations, see Figure 4.

4.3. Undulating Seafloor

The DBM reveals undulating seafloor topography on the central part of IT-A with knolls, sinks, ridges and smaller banks at depths ranging from 80 to 440 m (Figures 4 and 8). The knolls are defined by a round shape of 10–15 km in diameter and are elevated by more than 100 m compared to the surrounding bathymetry. They appear mainly in the southwestern part of the central IT-A, but a single knoll is located in IT-B (77.4°N, 16.7°W). Features of similar size but not round in shape are present in the east and northeast of the central IT-A (close about 79.5°N, 10°W). They show similar elevation changes as the knolls, but, in contrast, are elongate in shape, have relatively flat tops and an average depth shallower than 100 m. For these reasons, we have classified them as banks rather than knolls (Figure 8).

Sinks are abundant from about 81°N to 76.5°N on the middle shelf (Figures 4 and 8). The bottom of the sinks varies from 200 to 440 m in depth. In the southern middle shelf part of IT-A (around 78.3°N, 12°W), a shallower (approximately 170 m average water depth) and less intensively undulating area is present (Figures 4 and 8). Instead of showing pronounced knolls and sinks, the seafloor here is hummocky with irregularly undulating elevation changes of about 30 m on average.

The interpreted multichannel seismic profile AWI-99080 crosscuts several knolls and sinks on the undulating seafloor in the central IT-A area (Figures 4 and 9 for location). The data show subsurface structures down to 2–3 km in depth. Two types of seismic unit can be distinguished in the profile. Type I units are vertically oriented bodies with irregular internal reflectors. Three such bodies are visible in the data; the second reaches

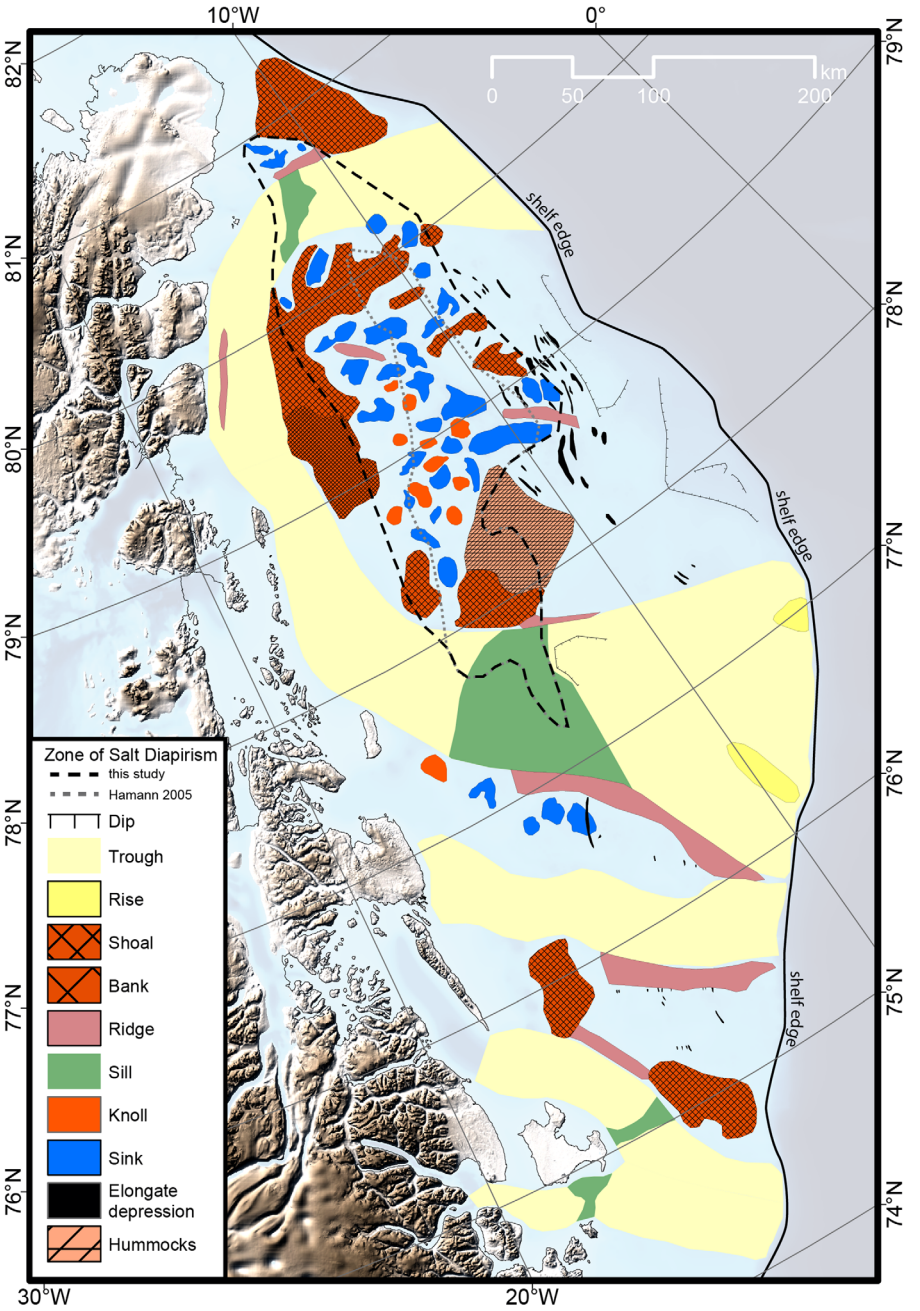

Figure 8. Schematic diagram of seafloor features on the Northeast Greenland continental shelf mapped from the digital bathymetric model.

the seafloor (Figure 9), whereas the other two are draped by Type II seismic units that, in contrast to Type I, have well-laminated internal reflectors. In the proximity of Type I seismic units, the reflectors of Type II units tend to bend upward with the distance between internal reflectors decreasing.

4.4. Middle Shelf Elongate Depressions

In a north-south strip on the eastern side of IT-A (between 10°W and 7°W), the NEG-DBM reveals the presence of elongate depressions (Figures 7a and 8). The depressions have a predominantly north-south orientation and often appear in close proximity to one another. They have U-shaped cross profiles. Compared to the adjacent seafloor, the depressions are on average 40 m deep with an average width of 1.5 km; ridges are present between depressions when they are located next to each other. Their maximum detected length is approximately 23 km. Accordingly, the minimum elongation ratio is approximately 1:15. Similar

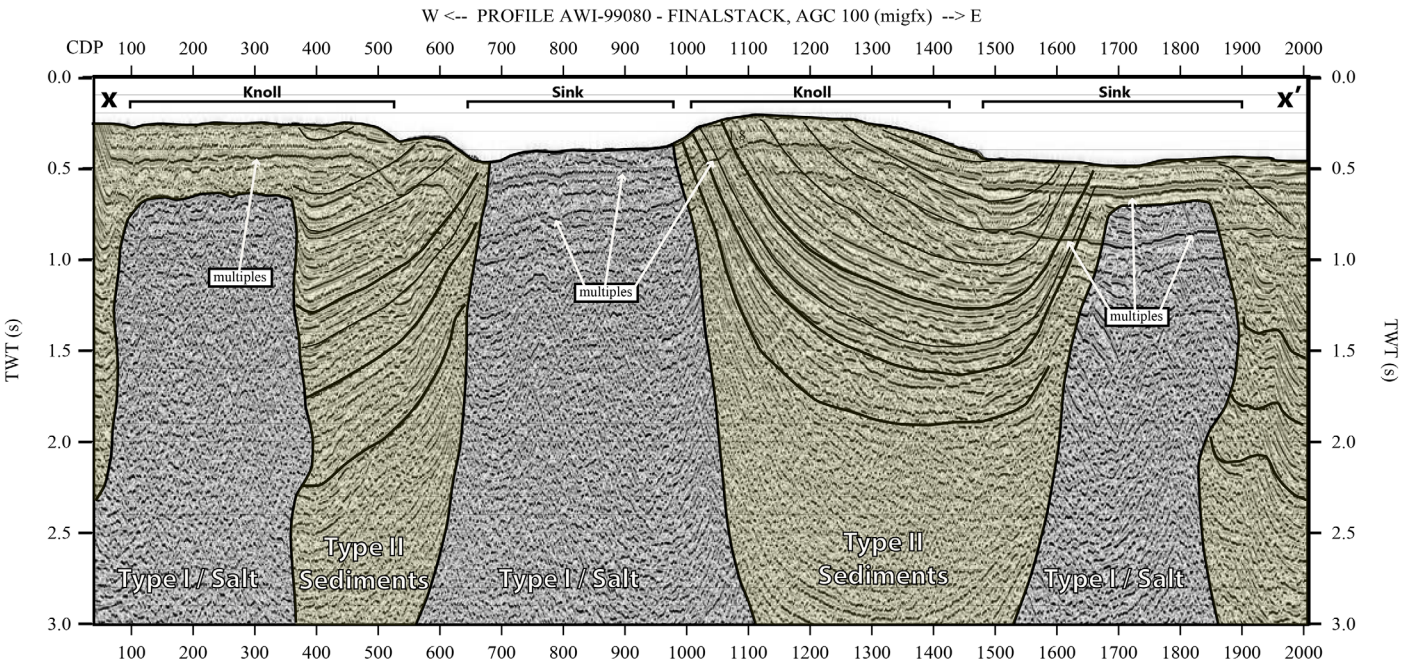

Figure 9. Seismic profile AWI-99080 crosscutting bathymetric knolls and sinks, showing that their formation is related to salt diapirism. For location, see Figure 4.

but much smaller elongate depressions are also present on the outer shelf of IT-B and IT-C (Figure 8). Hence, these elongate depressions are present from about 79°45′N to 75°15′N over a distance of approximately 500 km. No such features are detected in the cross-shelf troughs.

4.5. Fjords

Dijmphna Sund and Bredefjord (Figure 1) are the only coastal areas of the study area that are well covered by bathymetric soundings (Figure 2). In places, their depths are greater than 500 m. Most of the fjord bathymetry shows a relatively flat seafloor. Occasionally, however, their depth shallows abruptly to 100 m depth in Djimphna Sund and 150 m in Bredefjord within short distances. The other fjord systems are unconstrained by depth soundings, but the subaerial topography shows that they are surrounded mainly by the steep walls of adjacent mountains. In such locations, the fjords were modeled to 50 m water depth in the DBM with inferred contours (Figure 2).

The modern-day ice shelf of 79°-Glacier is located in a fjord (Nioghalvfjerdsfjorden; 79.5°N, 21°W) and is approximately 80 km long (Figure 4). The seafloor beneath the central part of the ice shelf is at about 900 m deep (Figure 5; 30–60 km), with an ice thickness of about 300 m and a water-filled cavity of about 600 m [*Mayer et al.*, 2000]. The northern ice front of 79°-Glacier terminates in Djimphna Sund at a maximum water depth of about 600 m. The eastern ice front is grounded on several ice rises and shows a shallower bathymetry with a maximum observed depth of about 250 m. The maximum depths of CTD stations, east of these ice rises (79.5°N, 19°W), show a deepening bathymetry. The next available depth information to the east is at 450 m water depth underneath the land-fast sea ice of the Norske Øer Ice Barrier (79.3°N, 17.5°W) [*Wadhams et al.*, 2006]. These few depth constraints suggest a deep (>250 m) representation of this very sparsely mapped area. Hence, we added inferred contours to model this area accordingly. The depths offshore of other glacier margins (Zachariae Isstrøm, Storstrømmen, and L. Bistrup Bræ; Figure 1b) have been manually steered down offshore of the ice front to the next reliable bedrock elevation present close to the ice front position.

5. Discussion

5.1. Digital Bathymetric Model

The new DBM of the NEG continental shelf is based on the most comprehensive and up to date data base of bathymetric soundings and other depth information of this area (Table 1). This made it reasonable to select a grid cell size of 250 m × 250 m, which is twice that of IBCAO Version 3.0 [*Jakobsson et al.*, 2012b]. The number of artifacts in the data set has been limited as much as possible by the iterative cleaning,

gridding and quality check steps (Figure 3). The combination of bathymetric data with bedrock topography data, instead of ice surface topography, and high-resolution land topography, has led to a smooth ocean-land transition in the DBM (Figure 4). In the new bathymetric model, submarine morphological features on the NEG continental shelf are now better resolved or revealed for the first time. Their description and interpretation improves our knowledge of processes taking place on the NEG continental shelf.

Despite the large data base of soundings, in some areas, data coverage is still sparse due mainly to year-round harsh sea-ice conditions linked to the cold East Greenland Current (Figure 1a). In these areas, the DBM suffers from reduced quality and reliability. This is most evident in areas close to the coast and in the vicinity of Norske Øer Ice Barrier (Figure 1), but also in a few parts of the continental shelf (Figure 2). The manually inferred contours attempt to give a realistic representation of the coastal bathymetry by estimating a continuation of the surrounding, better surveyed, bathymetry and topography. The inclusion of inferred contours at 50 m depth in major fjords based on neighboring steep fjord flanks yielded more realistic results than the otherwise <1 m deep fjords without manual steering. Nevertheless, we suggest that most of the fjords are probably several hundred meters deep, based on observations from elsewhere in Greenland [e.g., *Dowdeswell et al*., 2010, 2014], and require further detailed surveys.

5.2. Past Ice Flow

High-resolution swath-bathymetric data revealed the presence of mega-scale glacial lineations and recessional moraines in the middle shelf region of Westwind Trough (Figure 10) [*Evans et al*., 2009; *Winkelmann et al*., 2010]. These glacial-sedimentary landforms are produced subglacially and ice marginally, respectively, and provided the first direct seafloor geomorphological evidence for the expansion and presence of a grounded Greenland Ice Sheet on the NEG continental shelf during the late Quaternary. Furthermore, the presence of MSGL constrained to shelf trough areas indicates that this ice cover contained fast flowing ice streams that preferentially drained through these troughs. A review by *Funder et al*. [2011], utilizing the evidence from these two papers, suggested that the LGM Greenland Ice Sheet extended at least to the middle continental shelf of NEG (Figure 10). However, *Bennike and Björck* [2002] proposed that the Greenland Ice Sheet extended to the outer shelf, based on radiocarbon dates indicating late onshore deglaciation. This view is further supported by investigations of shallow sedimentary rocks along the East Greenland margin, which are predominantly of glacial origin [*Berger and Jokat*, 2008; *Berger and Jokat*, 2009; *García et al*., 2012; *Wilken and Mienert*, 2006]. Our new bathymetry reveals the presence of submarine features on the NEG continental shelf that we interpret to be formed by glacial processes. In addition, the presence of subglacial landforms and glacial sediments across the shoals and banks between troughs shows that they were probably influenced by grounded ice flow [*Evans et al*., 2009] and may have served as base for local marine ice domes that laterally constrained the direction of past ice flow within the troughs.

5.2.1. Cross-Shelf Troughs

Cross-shelf troughs are characteristic features of glaciated continental shelves [*Batchelor and Dowdeswell*, 2014]. The reverse slopes observed in the bathymetry of Westwind Trough, Norske Trough, Dove Bugt Trough, and Hochstetterbugten Trough are similar to overdeepened troughs present in other formerly ice-covered regions [*Batchelor and Dowdeswell*, 2014; *Livingstone et al*., 2012]. These troughs are suggested to be produced by high erosion rates beneath ice streams and rapid sediment transport to the ice-sheet margin during repeated glacial advances and retreats [*ten Brink and Schneider*, 1995]. Thus, this also suggests that the overdeepened troughs visible in the NEG bathymetry indicate ice-stream activity and subglacial erosion during multiple glaciations. Some of the ridges found on the edges of the glacial troughs are also similar in size and shape to lateral moraines found at the margins of other glacially eroded cross-shelf troughs [e.g., *Ottesen et al*., 2005]. This similarity is most obvious for the two pronounced ridges in Norske Trough (Figures 4 and 10). Accordingly, we interpret these ridges as lateral moraines that were produced during one or multiple glaciations, probably including the LGM, at the lateral shear margins of former ice streams [*Ottesen et al*., 2005; *Stokes and Clark*, 2002].

In contrast to the other troughs, Store Koldewey Trough has no reverse slope and the edges of the trough are not well pronounced (Figure 4). The ridge identified to the south of Store Koldewey Trough is broader and not as streamlined as those in the other troughs. The land topography implies that the interior ice-sheet basin-area draining into Store Koldewey Trough was much smaller than for the other troughs of the study area and that Store Koldewey Trough only served as a minor drainage path for the Greenland Ice Sheet (Figure 10). The mountain ranges between Germania Land and Storstrømmen Glacier (77.3°N, 21°W)

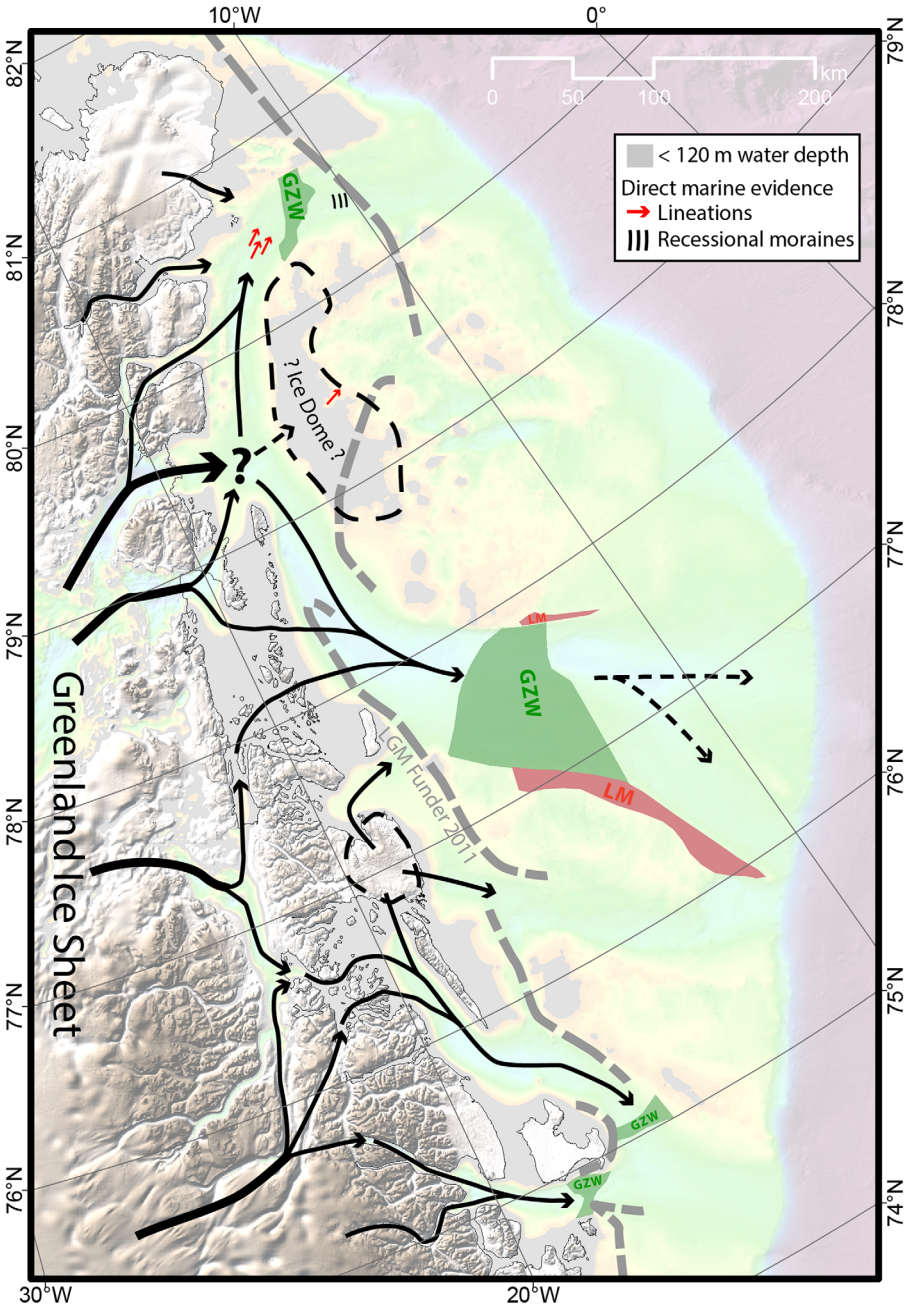

Figure 10. Interpretation of the paleo-ice flow on the Northeast Greenland shelf based on morphological features in the digital bathymetric model. Grounding-zone wedges (GZW, green) are located at similar distances from the modern-day fronts of marine-terminating outlet glaciers of the Greenland Ice Sheet. Lateral moraines (LM, red) are found at the sides of Norske Trough. Areas below 120 m water depth (grey) were above sea level at the LGM and could have supported an ice dome (black dashed line) built up on the shelf. The LGM ice extent across the shelf from *Funder et al.* [2011] is shown as grey dashed line.

provided a north to south trending obstacle for the Greenland Ice Sheet to drain in an eastward direction into Store Koldewey Trough (Figures 1b, 4, and 10). Instead, the north-south oriented fjord of Storstrømmen directs the outflow to Jøkelbugten in the north and Dove Bugt in the south (Figures 1b and 10). Thus, the drainage-basin area to Store Koldewey Trough is limited to Germania Land. The Germania Land topography suggests that major parts of its ice cover were drained to the north via Skærfjorden as a tributary to Norske Trough and to the south directly into Dove Bugt Trough (Figures 1b and 10), as also concluded from direct observations from Germania Land [*Landvik*, 1994]. Hence, we suggest that, in contrast to the other studied

troughs of NEG with reverse slopes, Store Koldewey Trough probably was not eroded by an ice stream during multiple glaciations.

5.2.2. Grounding-Zone Wedges

During still stands of the ice-sheet margin during regional deglacial retreat, the sediments transported to the terminus can build up sedimentary depositional centers, often referred to as grounding-zone wedges (GZWs) [e.g., *Batchelor and Dowdeswell*, 2015; *Dowdeswell and Fugelli*, 2012]. GZWs are asymmetrical, with a steeper ice-distal side and a longer but low-profile ice-proximal slope [e.g., *Ottesen et al*., 2007]. Typically, they appear as subdued ridges perpendicular to the ice-flow direction over the entire width of the ice stream [e.g., *Batchelor and Dowdeswell*, 2015; *Jakobsson et al*., 2012a]. The morphology of the bathymetric sills offshore of NEG shows great similarity to the typical morphology of GZWs (Figures 5a, 5b, 6b, 6c, and 7c). In addition, since they are located in glacial troughs, we interpret the sills in Westwind Trough, Norske Trough, Dove Bugt Trough, and Hochstetterbugten Trough as GZWs (Figure 10). All four GZWs are located on the middle shelf at a similar distance from the modern-day ice margin. Their locations are more or less in accordance with the proposed LGM position of the ice sheet at Westwind Trough, Dove Bugt Trough, and Hochstetterbugten Trough (Figure 10) [*Funder et al*., 2011]. The GZW found in Norske Trough is further offshore compared to the proposed LGM ice-sheet margin. *Batchelor and Dowdeswell* [2015] mapped 10 buried or seafloor GZWs in Norske Trough from seismic data, including a seafloor GZW on the outer shelf. Nine buried or near-seafloor GZWs have also been mapped using seismic records from Store Koldewey Trough [*Batchelor and Dowdeswell*, 2015]. Hence, the LGM position around Norske Trough was probably located further offshore than suggested by *Funder et al*. [2011].

5.2.3. Local Marine Ice Dome

Tuppiaq Qeqertaa (Tobias Island), located on the western edge of Northwind Shoal about 70 km off the NEG coast (Figure 1), is today covered by a small ice cap that rises to 35 m above sea level [*Bennike et al*., 2006]. The sea ice of the Norske Øer Ice Barrier develops each year around the island or around icebergs that ground in the shallow waters of Northwind Shoal [*Hughes et al*., 2011]. The shallow areas of the NEG shelf are clearly important in the buildup of landfast sea-ice today and, thus, may have acted as areas of initial buildup of marine-based ice sheets in the past [*Berger and Jokat*, 2009]. During LGM, global sea level was approximately 120 m lower than today [*Rohling et al*., 2009]. The DBM shows that large parts of the western IT-A are less than 120 m deep (Figure 10). Hence, under such conditions, the shoals and banks mapped on the DBM would have been emergent above sea level and could have served as bases of local marine ice dome, probably building up at the location of the modern-day small ice cap on Tobias Island (Figure 10).

Lavoie et al. [2015] investigated a bathymetric compilation around the Antarctic Peninsula and inferred the presence of seven local marine ice domes. These ice domes served as lateral constraints that guided the ice stream outlets. The planform of the Westwind Trough and Norske Trough centerlines indicates that ice flow draining across the shelf from the Greenland Ice Sheet was most likely redirected in a northward and southward direction around Northwind Shoal (Figure 10). Hence, we suggest that this redirection was probably constrained by an ice dome on NWS, similar to the ice domes suggested for the Antarctic Peninsula. *Evans et al*. [2009] showed that ice flow was active directly northeast of Northwind Shoal (Figure 10). Thus, assuming a complete redirection of the ice flow at Northwind Shoal as suggested by the trough morphology, the separate marine ice dome on the shoal was the source of this ice stream activity. Given an elevation above full-glacial sea level and an ice thickness large enough to initiate streaming ice, this ice dome could have harbored a significant contribution to sea level change. Using a rough calculation for ice dome thickness as used by *Lavoie et al*. [2015] with an estimated ice temperature of -20°C, a precipitation rate of $\sim$150 mm a^{-1} [*Ohmura and Reeh*, 1991], and an ice dome radius of 40–50 km yields an approximate thickness of 900 m in center of the dome. Estimating a more moderate ice thickness of 500 m for the entire inter-trough areas ($\sim$100,000 km^2) would yield an equivalent sea level rise of about 0.14 m; this contribution would clearly vary with the actual thickness and extent of glacier ice.

For verification of the ice dome presence, however, high-resolution bathymetric investigations of submarine glacial features in the area west of Northwind Shoalare necessary in order to determine if the ice flow from the Greenland Ice Sheet was crossing Northwind Shoalor if it was redirected into Westwind Trough and Norske Trough. However, the acquisition of such data has so far been impeded due to the persistence of the Norske Øer Ice Barrier.

5.2.4. Fjords

All fjord systems in our study area were covered by the Greenland Ice Sheet during the LGM and probably a number of previous glaciations, a pattern similar to that elsewhere in East Greenland [e.g., *Dowdeswell et al*., 2010, 1994b; *Evans et al*., 2002]. Thus, the deeply incised Dijmphna Sund and Bredefjord, as well as the other unsurveyed fjords in the area, are a result of glacial erosion from streaming ice that drained the expanded Greenland Ice Sheet during multiple Quaternary glaciations (Figure 10). Fjord systems can experience very high sediment accumulation rates, of up to 20 cm a^{-1}, when the ice is retreating, leading to sediment thicknesses of up to several hundred meters [e.g., *Hjelstuen et al*., 2009]. Thus, we interpret the flat seafloor in parts of Dijmphna Sund and Bredefjord as the uppermost layer of postglacial sediments that partially filled the deeply incised glacially eroded fjords after deglaciation. Predominantly, these sediments were transported to the fjord by glaciers and released at the ice-sheet margin or transported by drifting icebergs as observed in the more southerly Scoresby Sund [*Dowdeswell et al*., 1994a,; *Ó Cofaigh et al*., 2001; *Syvitski*, 1989]. However, it cannot be ruled out that the fjord sedimentary record also includes some fluvial and glacifluvial sediments that are transported along valleys in summer melting seasons in periods of a warmer climate and in modern conditions [*Hasholt*, 1996]. The steep rises and shallow intersections in fjord bathymetry are interpreted as bedrock outcrops [e.g., *Dowdeswell et al*., 2014].

5.3. Water Mass Pathways

Satellite observations have revealed recent ice loss from marine-terminating glaciers in NEG [*Helm et al*., 2014; *Khan et al*., 2014]. Studies from elsewhere in Greenland and Antarctica have showed that the rate of ice loss by basal melting at marine-terminating glaciers is linked to the flow of warm water masses to the glacier that enhance basal melting, especially where a floating ice shelf or ice tongue is present [*Christoffersen et al*., 2011; *Hellmer et al*., 2012; *Holland et al*., 2008; *Pritchard et al*., 2012]. Warm Atlantic water, providing energy for basal melting, is also observed in several fjords around Greenland, including the 79°-Glacier [*Straneo et al*., 2012]. The pathway of the water masses on the continental shelf is crucial for the temperature of this Atlantic water due to atmospheric heat loss and increased mixing with Polar Water at shallow locations [*Straneo et al*., 2012]. Cross-shelf troughs with a reversed bathymetry have been demonstrated elsewhere to act as deep pathways that can direct warmer water into ice-shelf cavities, enhancing basal melting [*Hellmer et al*., 2012; *Walker et al*., 2007]. By contrast, bathymetric sills in a trough can also stabilize a retreating ice sheet in times of global warming by preventing the inflow of warmer water masses to the ice-sheet margin [*Jenkins et al*., 2010] and also by acting as pinning points and reducing iceberg production in relatively shallow water. Thus, the bathymetry of the cross-shelf troughs, fjords, and their sills is a key parameter for modeling the water mass exchange from the ocean to the glaciers and its impact on basal melting. The DBM reveals that all four major marine-terminating glaciers in the survey area (79°-Glacier, Zachariae Isstrøm, Storstrømmen, and L. Bistrup Bræ; Figure 1) are located at the western end of cross-shelf troughs with a reverse slope in bathymetry (Figure 4) that would allow the inflow of warm water to the ice front. Bathymetric sills in the troughs on the shelf and the fjord systems are obstacles in this pathway. The DBM defines these features and serves as an important morphological boundary condition for oceanographic modeling.

5.4. Halokinesis

The spatial distribution of knolls, sinks, and hummocky seafloor on the continental shelf of NEG (Figure 8) shows strong congruence to the previously mapped area of salt diapirism [*Hamann et al*., 2005]. Seismic line AWI-99080 crosses knolls and sinks in the central IT-A area (Figure 4). We interpret acoustic unit Type I as uplifted salt structures (Figure 9). Occasionally, these salt structures crop out at the seafloor (Figure 9). Here they can be dissolved by seawater and form sinks. The sedimentary layers between the salt bodies (acoustic unit Type II) are synclinal in form and thin toward the salt bodies. The seafloor reflector of the seismic line demonstrates that the undulating seafloor topography in this area is influenced by the salt tectonics active beneath (Figure 9). Synclinal reflectors in the top sedimentary layers have also been identified in subbottom profiler data in the northern part of IT-A [*Evans et al*., 2009]. These reflectors were linked to subaqueous sediment gravity flows at an ice-sheet margin or to glacitectonism of older unconsolidated sediments after an ice advance. The similarity of the top reflectors visible in the subbottom profiler data to those visible in the seismic data, however, suggests that both were caused by salt tectonics. Hence, we conclude that the undulating seafloor topography, where knolls, sinks, and hummocky seafloor were mapped from the DBM, is most probably related to salt diapirism active underneath. Accordingly, we suggest that

the area of salt tectonic activity is larger than previously estimated at approximately 33,000 km^2 (Figure 8), extending further to the northwest than the previously estimated area, which was based on a limited number of seismic lines (Figure 8) [*Hamann et al*., 2005].

5.5. Elongate Depressions

The mainly north-south trending elongate depressions on the middle to outer shelf of NEG, illustrated in Figure 7a and mapped in Figure 8, were only detected in areas with relatively dense bathymetric data coverage (Figure 2). The reduced length of the more southerly elongate depressions is likely due to the lower coverage with high-resolution sounding data in that area. Here additional elongate depressions are probably present on the continental shelf but remain unresolved in the DBM.

The elongate depressions appear in basins filled with several kilometer-thick sediments [*Hamann et al*., 2005]. They are located in the area of the north to south flowing EGC. While the major part of the EGC flows through the deeper western part of Fram Strait and along the continental slope, the EGC also flows over the middle to outer shelf of NEG at about 79°N and 8°W. Here a steady north to south water flow has been observed [*Bourke et al*., 1987; *Budéus and Schneider*, 1995; *Rabe et al*., 2009]. On the inner shelf, where no elongate depressions have been found, the currents are relatively less intense and show more fluctuations [*Bourke et al*., 1987; *Budéus and Schneider*, 1995; *Wadhams et al*., 2006]. The location of the elongate depressions could coincide with a full-glacial ice margin close to the shelf edge. If this is so, the depressions could have been formed by ice-marginal processes, possibly in combination with erosion caused by the EGC. The depressions may have formed: (a) between ice-marginal sedimentary deposition centers or are landforms produced by proglacial and submarginal glacitectonics, e.g., moraines or composite ridges [*Benn and Evans*, 2010] or (b) by a strengthened EGC that eroded sediments along a stable past ice margin, similar to moat structures at the base of continental slopes [*Rebesco et al*., 2014]. The absence of elongate depressions in the cross-shelf troughs of NEG may be due to the presence of overconsolidated sediments, caused by ice flow in the troughs, that are less prone to erosional forces than noncompacted sediments. A systematic high-resolution bathymetric survey of the elongate depressions in combination of shallow seismic data acquisition across the depressions is needed to verify our interpretation.

5.6. Volcanic Remnants

The flat-topped peak at the bathymetric sill in Hochstetterbugten Trough south of Shannon Island is interpreted to be of volcanic origin (Figure 7b). The NEG volcanic province stretches from 75°N to 72°N of the continental shelf [*Hamann et al*., 2005]. Eastern Shannon Island, 30 km north of the peak, and Pendulum Øer, 20 km south of the peak (Figure 7b), consist of basalts [*Henriksen*, 2003]. *Voss et al*. [2009] observed a significant seismic-velocity anomaly at the location of the peak. They also found no significant high-velocity lower crust which, in contrast, was observed further south, and that a positive magnetic anomaly is present at this location. They concluded that the observed surface basalts were related to a local volcanic event. We interpret the outcropping peak in the DBM as a remnant of this volcanic event. Eruption rates of the North Atlantic Igneous Province were highest between 56 and 55 Ma and later on were active only at the East Greenland margin between 66°N and 69°N [*Storey et al*., 2007]. Assuming 55 Ma as the timing of the volcanic event, the guyot-like flat top of the peak at 250 m water depth is most probably a result of subsequent erosion by waves together with erosion by ice during glaciations.

6. Conclusions

The new DBM of the NEG continental shelf shown in Figure 4 has improved our knowledge of the shelf bathymetry compared to previous maps and models. The detailed grid allows the identification of seafloor features that have not been mapped previously or have had their shape insufficiently resolved. Nevertheless, the coverage map reveals that parts of the NEG shelf, especially close to the coast (Figure 2), are still not or only sparsely covered by soundings and additional data are needed to further improve our description and understanding of the NEG shelf.

The DBM reveals that the shape of the NEG continental shelf has been affected by a number of processes, including glacial erosion and deposition, salt tectonics (halokinesis), and past volcanism. The cross-shelf troughs were formed by glacial erosion by ice streams that drained an expanded Greenland Ice Sheet in full-glacial periods (Figure 10). Under modern conditions, these troughs act as potential pathways for

relatively warm Atlantic waters to flow across the shelf to the margins of the marine-terminating glaciers and beneath any floating ice. Bathymetric sills (Figures 7c and 8), located in the cross-shelf troughs, are interpreted as depositional grounding-zone wedges that formed at the ice margin during phases of prolonged ice-sheet still stand (Figure 10), probably during deglaciation from the LGM. Salt tectonics formed the irregular seafloor on much of the middle shelf, represented by pronounced knolls, sinks, and hummocky areas (Figure 8). North-south trending elongate depressions have been mapped between the cross-shelf troughs on the middle to outer shelf (Figures 7a and 8). They are probably related to ice-marginal processes and ocean currents. In central Hochstetter Bugten Trough, a guyot-like remnant of a former volcano has been detected (Figure 7b), which is linked to a single volcanic event that probably occurred 55 Ma ago. The DBM can be obtained from http://dx.doi.org/10.1594/PANGAEA.849313.

Acknowledgments

We thank crew and scientists onboard of each data contributing cruise. We thank TGS for contributing depth information along their seismic lines. We thank Paul Dodd from the Norske Polar Institut, Martin Jakobsson from Stockholm University, and Fiamma Straneo from Woods Hole Oceanographic Institution for their contributions of echo sounder data. We thank Peter Wadhams who was chief scientist of JR106 and Autosub-II leg M365. We thank E. Domack and one anonymous reviewer for providing helpful comments on a previous version of this publication.

References

Aagaard, K., and L. K. Coachman (1968), The East Greenland current north of Denmark Strait: Part I, *Arctic*, *21*, 181–200.

Arndt, J. E., et al. (2013), The International Bathymetric Chart of the Southern Ocean (IBCSO) Version 1.0—A new bathymetric compilation covering circum-Antarctic waters, *Geophys. Res. Lett.*, *40*, 3111–3117, doi:10.1002/grl.50413.

Batchelor, C. L., and J. A. Dowdeswell (2014), The physiography of High Arctic cross-shelf troughs, *Quat. Sci. Rev.*, *92*, 68–96, doi:10.1016/j.quascirev.2013.05.025.

Batchelor, C. L., and J. A. Dowdeswell (2015), Ice-sheet grounding-zone wedges (GZWs) on high-latitude continental margins, *Mar. Geol.*, *363*, 65–92, doi:10.1016/j.margeo.2015.02.001.

Benn, D. I., and D. J. A. Evans (2010), *Glaciers & Glaciation*, 2nd ed., Hodder Educ., London, U. K.

Bennike, O., and S. Björck (2002), Chronology of the last recession of the Greenland Ice Sheet, *J. Quat. Sci.*, *17*(3), 211–219, doi:10.1002/jqs.670.

Bennike, O., and A. Weidick (2001), Late Quaternary history around Nioghalvfjerdsfjorden and Jøkelbugten, North-East Greenland, *Boreas*, *30*(3), 205–227, doi:10.1111/j.1502-3885.2001.tb01223.x.

Bennike, O., N. Mikkelsen, R. Forsberg, and L. Hedenas (2006), Tuppiap Qeqertaa (Tobias Island): A newly discovered island off northeast Greenland, *Polar Record*, *42*(223), 309–314.

Berger, D., and W. Jokat (2008), A seismic study along the East Greenland margin from 72°N to 77°N, *Geophys. J. Int.*, *174*(2), 733–748, doi:10.1111/j.1365-246X.2008.03794.x.

Berger, D., and W. Jokat (2009), Sediment deposition in the northern basins of the North Atlantic and characteristic variations in shelf sedimentation along the East Greenland margin, *Mar. Pet. Geol.*, *26*(8), 1321–1337, doi:10.1016/j.marpetgeo.2009.04.005.

Bourke, R. H., J. L. Newton, R. G. Paquette, and M. D. Tunnicliffe (1987), Circulation and water masses of the East Greenland shelf, *J. Geophys. Res.*, *92*(C7), 6729–6740, doi:10.1029/JC092iC07p06729.

Budéus, G., and W. Schneider (1995), On the hydrography of the Northeast Water Polynya, *J. Geophys. Res.*, *100*(C3), 4287–4299, doi:10.1029/94JC02024.

Cherkis, N., and P. R. Vogt (1994), *Regional Bathymetry of the Northern Norwegian—Greenland Sea*, Nav. Res. Lab., Washington, D. C.

Christoffersen, P., R. I. Mugford, K. J. Heywood, I. Joughin, J. A. Dowdeswell, J. P. M. Syvitski, A. Luckman, and T. J. Benham (2011), Warming of waters in an East Greenland fjord prior to glacier retreat: Mechanisms and connection to large-scale atmospheric conditions, *Cryosphere*, *5*(3), 701–714, doi:10.5194/tc-5-701-2011.

Dickens, W. A., A. G. C. Graham, J. A. Smith, J. A. Dowdeswell, R. D. Larter, C.-D. Hillenbrand, P. N. Trathan, J. E. Arndt, and G. Kuhn (2014), A new bathymetric compilation for the South Orkney Islands region, Antarctic Peninsula (49°–39°W to 64°–59°S): Insights into the glacial development of the continental shelf, *Geochem. Geophys. Geosyst.*, *15*, 2494–2514, doi:10.1002/2014GC005323.

Dowdeswell, J. A., and E. M. G. Fugelli (2012), The seismic architecture and geometry of grounding-zone wedges formed at the marine margins of past ice sheets, *Geol. Soc. Am. Bull.*, *124*(11-12), 1750, doi:10.1130/B30628.1.

Dowdeswell, J. A., R. J. Whittington, and P. Marienfeld (1994a), The origin of massive diamicton facies by iceberg rafting and scouring, Scoresby Sund, East Greenland, *Sedimentology*, *41*(1), 21–35, doi:10.1111/j.1365-3091.1994.tb01390.x.

Dowdeswell, J. A., G. Uenzelmann-Neben, R. J. Whittington, and P. Marienfeld (1994b), The Late Quaternary sedimentary record in Scoresby Sund, East Greenland, *Boreas*, *23*(4), 294–310, doi:10.1111/j.1502-3885.1994.tb00602.x.

Dowdeswell, J. A., R. J. Whittington, A. E. Jennings, J. T. Andrews, A. Mackensen, and P. Marienfeld (2000), An origin for laminated glacimarine sediments through sea-ice build-up and suppressed iceberg rafting, *Sedimentology*, *47*(3), 557–576, doi:10.1046/j.1365-3091.2000.00306.x.

Dowdeswell, J. A., J. Evans, and C. Ó Cofaigh (2010), Submarine landforms and shallow acoustic stratigraphy of a 400 km-long fjord-shelf-slope transect, Kangerlussuaq margin, East Greenland, *Quat. Sci. Rev.*, *29*(25–26), 3359–3369, doi:10.1016/j.quascirev.2010.06.006.

Dowdeswell, J. A., K. A. Hogan, C. Ó Cofaigh, E. M. G. Fugelli, J. Evans, and R. Noormets (2014), Late Quaternary ice flow in a West Greenland fjord and cross-shelf trough system: Submarine landforms from Rink Isbrae to Uummannaq shelf and slope, *Quat. Sci. Rev.*, *92*, 292–309, doi:10.1016/j.quascirev.2013.09.007.

Engen, Ø., J. I. Faleide, and T. K. Dyreng (2008), Opening of the Fram Strait gateway: A review of plate tectonic constraints, *Tectonophysics*, *450*(1–4), 51–69, doi:10.1016/j.tecto.2008.01.002.

Evans, J., J. A. Dowdeswell, H. Grobe, F. Niessen, R. Stein, H.-W. Hubberten, and R. J. Whittington (2002), Late Quaternary sedimentation in Kejser Franz Joseph Fjord and the continental margin of East Greenland, *Geol. Soc. Spec. Publ.*, *203*(1), 149–179, doi:10.1144/GSL.SP.2002.203.01.09.

Evans, J., C. Ó Cofaigh, J. A. Dowdeswell, and P. Wadhams (2009), Marine geophysical evidence for former expansion and flow of the Greenland Ice Sheet across the north-east Greenland continental shelf, *J. Quat. Sci.*, *24*(3), 279–293, doi:10.1002/jqs.1231.

Funder, S., K. K. Kjeldsen, K. H. Kjær, and C. Ó Cofaigh (2011), The Greenland Ice Sheet during the past 300,000 years: A review, in *Quaternary Glaciations—Extent and Chronology*, edited by J. Ehlers, P. L. Gibbard, and P. D. Hughes, pp. 699–713, Elsevier, Amsterdam.

García, M., J. A. Dowdeswell, G. Ercilla, and M. Jakobsson (2012), Recent glacially influenced sedimentary processes on the East Greenland continental slope and deep Greenland Basin, *Quat. Sci. Rev.*, *49*, 64–81, doi:10.1016/j.quascirev.2012.06.016.

Graham, A. G. C., F. O. Nitsche, and R. D. Larter (2011), An improved bathymetry compilation for the Bellingshausen Sea, Antarctica, to inform ice-sheet and ocean models, *Cryosphere*, *5*, 95–106, doi:10.5194/tc-5-95-2011.

Hamann, N. E., R. C. Whittaker, and L. Stemmerik (2005), Geological development of the Northeast Greenland Shelf, *Pet. Geol. Conf. Ser.*, *6*, 887–902, doi:10.1144/0060887.
Hasholt, B. (1996), Sediment transport in Greenland, in *Erosion and Sediment Yield: Global and Regional Perspectives*, edited by D. E. Walling and B. Webb, pp. 105–114, IAHS Press, Wallingford, U. K.
Hell, B., and M. Jakobsson (2011), Gridding heterogeneuos bathymetric data sets with stacked continous curvature splines in tension, *Mar. Geophys. Res.*, *32*(4), 493–501, doi:10.1007/s11001-011-9141-1.
Hellmer, H. H., F. Kauker, R. Timmermann, J. Determann, and J. Rae (2012), Twenty-first-century warming of a large Antarctic ice-shelf cavity by a redirected coastal current, *Nature*, *485*, 225–228, doi:10.1038/nature11064.
Helm, V., A. Humbert, and H. Miller (2014), Elevation and elevation change of Greenland and Antarctica derived from CryoSat-2, *Cryosphere*, *8*(4), 1539–1559, doi:10.5194/tc-8-1539-2014.
Henriksen, N. (2003), *Caledonian Orogen East Greenland 70° - 82° N*, Geol. Surv. of Den. and Greenl., Copenhagen.
Hjelstuen, B. O., H. Haflidason, H. P. Sejrup, and A. Lyså (2009), Sedimentary processes and depositional environments in glaciated fjord systems—Evidence from Nordfjord, Norway, *Mar. Geol.*, *258*(1–4), 88–99, doi:10.1016/j.margeo.2008.11.010.
Holland, D. M., R. H. Thomas, B. de Young, M. H. Ribergaard, and B. Lyberth (2008), Acceleration of Jakobshavn Isbrae triggered by warm subsurface ocean waters, *Nat. Geosci.*, *1*(10), 659–664, doi:10.1038/ngeo316.
Howat, I. M., A. Negrete, and B. E. Smith (2014), The Greenland Ice Mapping Project (GIMP) land classification and surface elevation data sets, *Cryosphere*, *8*(4), 1509–1518, doi:10.5194/tc-8-1509-2014.
Hughes, N. E., J. P. Wilkinson, and P. Wadhams (2011), Multi-satellite sensor analysis of fast-ice development in the Norske Øer Ice Barrier, northeast Greenland, *Ann. Glaciol.*, *52*(57), 151–160.
Jakobsson, M., C. Marcussen, and S. P. Lomrog (2008), Lomonosov Ridge off Greenland 2007 (LOMROG)—Cruise report, report, 122 pp., Geol. Surv. of Den. and Greenl., Copenhagen.
Jakobsson, M., et al. (2010), An Arctic Ocean ice shelf during MIS 6 constrained by new geophysical and geological data, *Quaternary Science Reviews*, *29*, 3505–3517, doi:10.1016/j.quascirev.2010.03.015.
Jakobsson, M., J. B. Anderson, F. O. Nitsche, R. Gyllencreutz, A. E. Kirshner, N. Kirchner, M. O'Regan, R. Mohammad, and B. Eriksson (2012a), Ice sheet retreat dynamics inferred from glacial morphology of the central Pine Island Bay Trough, West Antarctica, *Quat. Sci. Rev.*, *38*, 1–10, doi:10.1016/j.quascirev.2011.12.017.
Jakobsson, M., et al. (2012b), The International Bathymetric Chart of the Arctic Ocean (IBCAO) Version 3.0, *Geophys. Res. Lett.*, *39*, L12609, doi:10.1029/2012GL052219.
Jenkins, A., P. Dutrieux, S. S. Jacobs, S. McPhail, J. R. Perrett, A. T. Webb, and D. White (2010), Observations beneath Pine Island Glacier in West Antarctica and implications for its retreat, *Nat. Geosci.*, *3*, 468–472, doi:10.1038/ngeo890.
Johnson, G. L., and O. B. Eckhoff (1966), Bathymetry of the north Greenland Sea, *Deep Sea Res. Oceanogr. Abstr.*, *13*(6), 1161–1173, doi:10.1016/0011-7471(66)90707-8.
Joughin, I., M. Fahnestock, D. MacAyeal, J. L. Bamber, and P. Gogineni (2001), Observation and analysis of ice flow in the largest Greenland ice stream, *J. Geophys. Res.*, *106*(D24), 34,021-34,034, doi:10.1029/2001JD900087.
Joughin, I., B. E. Smith, I. M. Howat, T. Scambos, and T. Moon (2010), Greenland flow variability from ice-sheet-wide velocity mapping, *J. Glaciol.*, *56*(197), 415–430, doi:10.3189/002214310792447734.
Khan, S. A., et al. (2014), Sustained mass loss of the northeast Greenland ice sheet triggered by regional warming, *Nat. Clim. Change*, *4*(4), 292–299, doi:10.1038/nclimate2161.
Klenke, M., and H. W. Schenke (2002), A new bathymetric model for the central Fram Strait, Mar. Geophys. Res., *23*, 367–378.
Landvik, J. Y. (1994), The last glaciation of Germania Land and adjacent areas, northeast Greenland, *J. Quat. Sci.*, *9*(1), 81–92, doi:10.1002/jqs.3390090108.
Lavoie, C., et al. (2015), Configuration of the Northern Antarctic Peninsula Ice Sheet at LGM based on a new synthesis of seabed imagery, *Cryosphere*, *9*(2), 613–629, doi:10.5194/tc-9-613-2015.
Livingstone, S. J., C. Ó Cofaigh, C. R. Stokes, C.-D. Hillenbrand, A. Vieli, and S. S. R. Jamieson (2012), Antarctic palaeo-ice streams, *Earth Sci. Rev.*, *111*(1–2), 90–128, doi:10.1016/j.earscirev.2011.10.003.
Mayer, C., N. Reeh, F. Jung-Rothenhäusler, P. Huybrechts, and H. Oerter (2000), The subglacial cavity and implied dynamics under Nioghalvfjerdsfjorden Glacier, NE-Greenland, *Geophys. Res. Lett.*, *27*(15), 2289–2292, doi:10.1029/2000GL011514.
Morlighem, M., E. Rignot, J. Mouginot, H. Seroussi, and E. Larour (2014), Deeply incised submarine glacial valleys beneath the Greenland ice sheet, *Nat. Geosci.*, *7*(6), 418–422, doi:10.1038/ngeo2167.
NASA Landsat Program (2000), *L7CPF20000701_20000718_08—Orthorectified*, edited by Landsat7, U.S. Geol. Surv., Sioux Falls, S. D.
Nitsche, F. O., S. S. Jacobs, R. D. Larter, and K. Gohl (2007), Bathymetry of the Amundsen Sea continental shelf: Implications for geology, oceanography, and glaciology, *Geochem. Geophys. Geosyst.*, *8*, Q10009, doi:10.1029/2007GC001694.
Ó Cofaigh, C., J. A. Dowdeswell, and H. Grobe (2001), Holocene glacimarine sedimentation, inner Scoresby Sund, East Greenland: The influence of fast-flowing ice-sheet outlet glaciers, *Mar. Geol.*, *175*(1–4), 103–129, doi:10.1016/S0025-3227(01)00117-7.
Ohmura, A., and N. Reeh (1991), New precipitation and accumulation maps for Greenland, *J. Glaciol.*, *37*(125), 140–148.
Ottesen, D., J. A. Dowdeswell, and L. Rise (2005), Submarine landforms and the reconstruction of fast-flowing ice streams within a large Quaternary ice sheet: The 2500-km-long Norwegian-Svalbard margin (57°–80°N), *GSA Bull.*, *117*(7–8), 1033–1050, doi:10.1130/B25577.1.
Ottesen, D., J. A. Dowdeswell, J. Y. Landvik, and J. Mienert (2007), Dynamics of the Late Weichselian ice sheet on Svalbard inferred from high-resolution sea-floor morphology, *Boreas*, *36*(3), 286–306, doi:10.1080/03009480701210378.
Perry, R. K., H. S. Fleming, N. Cherkis, R. H. Feden, and P. R. Vogt (1980), Bathymetry of the Norwegian-Greenland and western Barents seas, chart, U.S. Nav. Res. Lab., Washington, D. C.
Pritchard, H. D., S. R. M. Ligtenberg, H. A. Fricker, D. G. Vaughan, M. R. van den Broeke, and L. Padman (2012), Antarctic ice-sheet loss driven by basal melting of ice shelves, *Nature*, *484*, 502–505, doi:10.1038/nature10968.
Rabe, B., U. Schauer, A. Mackensen, M. Karcher, E. Hansen, and A. Beszczynska-Möller (2009), Freshwater components and transports in the Fram Strait—Recent observations and changes since the late 1990s, *Ocean Sci.*, *5*(3), 219–233, doi:10.5194/os-5-219-2009.
Rebesco, M., F. J. Hernández-Molina, D. Van Rooij, and A. Wåhlin (2014), Contourites and associated sediments controlled by deep-water circulation processes: State-of-the-art and future considerations, *Mar. Geol.*, *352*, 111–154, doi:10.1016/j.margeo.2014.03.011.
Rignot, E., and P. Kanagaratnam (2006), Changes in the velocity structure of the Greenland Ice Sheet, *Science*, *311*(5763), 986–990, doi:10.1126/science.1121381.
Rohling, E. J., K. Grant, M. Bolshaw, A. P. Roberts, M. Siddall, C. Hemleben, and M. Kucera (2009), Antarctic temperature and global sea level closely coupled over the past five glacial cycles, *Nat. Geosci.*, *2*(7), 500–504, doi:10.1038/ngeo557.

Smith, W. H. F., and P. Wessel (1990), Gridding with continuous curvature splines in tension, *Geophysics*, *55*(3), 293–305, doi:10.1190/1.1442837.

Stokes, C. R., and C. D. Clark (2002), Ice stream shear margin moraines, *Earth Surf. Processes Landforms*, *27*(5), 547–558, doi:10.1002/esp.326.

Storey, M., R. A. Duncan, and C. Tegner (2007), Timing and duration of volcanism in the North Atlantic Igneous Province: Implications for geodynamics and links to the Iceland hotspot, *Chem. Geol.*, *241*(3–4), 264–281, doi:10.1016/j.chemgeo.2007.01.016.

Straneo, F., D. A. Sutherland, D. Holland, C. Gladish, G. S. Hamilton, H. L. Johnson, E. Rignot, Y. Xu, and M. Koppes (2012), Characteristics of ocean waters reaching Greenland's glaciers, *Ann. Glaciol.*, *53*(60), 202–210.

Syvitski, J. P. M. (1989), On the deposition of sediment within glacier-influenced fjords: Oceanographic controls, *Mar. Geol.*, *85*(2–4), 301–329, doi:10.1016/0025-3227(89)90158-8.

ten Brink, U. S., and C. Schneider (1995), Glacial morphology and depositional sequences of the Antarctic continental shelf, *Geology*, *23*(7), 580–584, doi:10.1130/0091-7613(1995)023 < 0580:GMADSO > 2.3.CO;2.

Voss, M., M. C. Schmidt-Aursch, and W. Jokat (2009), Variations in magmatic processes along the East Greenland volcanic margin, *Geophys. J. Int.*, *177*(2), 755–782, doi:10.1111/j.1365-246X.2009.04077.x.

Wadhams, P., J. P. Wilkinson, and S. D. McPhail (2006), A new view of the underside of Arctic sea ice, *Geophys. Res. Lett.*, *33*, L04501, doi:10.1029/2005GL025131.

Walker, D. P., M. A. Brandon, A. Jenkins, J. T. Allen, J. A. Dowdeswell, and J. Evans (2007), Oceanic heat transport onto Amundsen Sea shelf through a submarine glacial trough, *Geophys. Res. Lett.*, *34*, L02602, doi:10.1029/2006GL028154.

Wilken, M., and J. Mienert (2006), Submarine glacigenic debris flows, deep-sea channels and past ice-stream behaviour of the East Greenland continental margin, *Quat. Sci. Rev.*, *25*(7–8), 784–810, doi:10.1016/j.quascirev.2005.06.004.

Winkelmann, D., W. Jokat, L. Jensen, and H.-W. Schenke (2010), Submarine end moraines on the continental shelf off NE Greenland—Implications for Lateglacial dynamics, *Quat. Sci. Rev.*, *29*, 1069–1077, doi:10.1016/j.quascirev.2010.02.002.

Zwally, H. J., M. B. Giovinetto, M. A. Beckley, and J. L. Saba (2012), *Antarctic and Greenland Drainage Systems*, GSFC Cryospheric Sciences Laboratory.